SF 298 MASTER COPY KEEP THIS COPY FOR REPRODUCTION PURPOSES

REPORT DOCUMENTATION PAGE

Form Approved
OMB NO. 0704-0188

1. AGENCY USE ONLY *(Leave blank)*	2. REPORT DATE	3. REPORT TYPE AND DATES COVERED
	September 28, 2001	01 Apr 95 - 30 Sep 01 Final Report

4. TITLE AND SUBTITLE

Comprehensive Evaluation of Catalytic Hydroreduction and Nonthermal Plasma as Alternative Technologies for Detoxification of Chemical Wastes

5. FUNDING NUMBERS

DAAH04-95-K-0001

6. AUTHOR(S)

B.W.-L. Jang; J.J. Spivey; C.R. Savage; and R.B. Timmons

7. PERFORMING ORGANIZATION NAMES(S) AND ADDRESS(ES)

Research Triangle Institute (RTI)
P. O. Box 12194
Research Triangle Park, NC 27709-2194

8. PERFORMING ORGANIZATION REPORT NUMBER

9. SPONSORING / MONITORING AGENCY NAME(S) AND ADDRESS(ES)

U.S. Army Research Office
P.O. Box 12211
Research Triangle Park, NC 27709-2211

10. SPONSORING / MONITORING AGENCY REPORT NUMBER

34523.6-CH-ERI

11. SUPPLEMENTARY NOTES

The views, opinions and/or findings contained in this report are those of the author(s) and should not be construed as an official Department of the Army position, policy or decision, unless so designated by other documentation.

12a. DISTRIBUTION / AVAILABILITY STATEMENT

Approved for public release; distribution unlimited.

12 b. DISTRIBUTION CODE

13. ABSTRACT *(Maximum 200 words)*

The longevity of the catalytic hydrotreatment of chloroethyl ethyl sulfide has been demonstrated over Ni-Mo/AC and Pt/MZ391 catalysts. 99.996% to 99.999% destruction efficiency was achieved. The results suggest that catalytic Hydrotreatment is a promising technology for the detoxification of mustard gas.

The RF non-thermal plasma technology has been successfully demonstrated to be effective for the removal and destruction of DNT, TNT, RDX, and Comp B on shell surfaces. Destruction and removal efficiency above 99.99% was achieved for most of the tests. N_2, CO_2, and H_2O are the major decontamination products with small amounts of No_x, mainly NO, generated. The process is economical and environmentally benign. It is estimated that the current nondestructive decontamination process can be scaled up to decontaminate shell casings at an operating cost of less than $30/metric ton.

14. SUBJECT TERMS

Catalyst, hydrotreatment, chemical agent, plasma, explosive, decontamination, and surface treatment.

15. NUMBER OF PAGES

51

16. PRICE CODE

17. SECURITY CLASSIFICATION OR REPORT	18. SECURITY CLASSIFICATION OF THIS PAGE	19. SECURITY CLASSIFICATION OF ABSTRACT	20. LIMITATION OF ABSTRACT
UNCLASSIFIED	UNCLASSIFIED	UNCLASSIFIED	UL

COMPREHENSIVE EVALUATION OF CATALYTIC HYDROREDUCTION AND NONTHERMAL PLASMA AS ALTERNATIVE TECHNOLOGIES FOR DETOXIFICATION OF CHEMICAL WASTES

FINAL REPORT

B.W.-L. Jang
J.J. Spivey
C.R. Savage
R.B. Timmons

September 2001

U.S. Army Research Office

CONTRACT NO. DAAH04-95-K-0001

Research Triangle Institute
P.O. Box 12194
Research Triangle Park, NC 27709-2194

RTI
INTERNATIONAL

TABLE OF CONTENTS

LIST OF FIGURES

List of Figures (Continued)

LIST OF TABLES

1.0 BACKGROUND

1.1 HYDROTREATMENT OF CHEMICAL WASTES

There are about 25,000 tons of chemical warfare (CW) agents in the U.S. stockpile [1]. About 90% of this stockpile must be destroyed by 2004 according to a public law enacted by Congress [2]. At present, the major disposal routes for these materials involve incineration processes. However, it is extremely difficult to achieve complete destruction of these wastes without producing noxious byproducts. Although some of the byproduct production could be decreased via even finer control of oxidation conditions and/or by post-burn procedures, these improvements would add substantially to the already high cost of waste disposal.

This investigation focused on the development of an environmentally acceptable route of reductive catalytic disposal in lieu of the oxidative method currently used to detoxify CW agents. We investigated catalytic hydrogenation of chloroethyl ethyl sulfide (CEES), a simulant of HD (mustard gas), to explore the potential of the reductive approach as an alternative way to dispose of the stockpile. The thermodynamics of the hydrogenation process are highly favorable. Furthermore, in sharp contrast with most oxidative destruction procedures, the reaction products from the reductive conversions (namely, hydrocarbons and hydrogen sulfide and hydrogen halides) not only pose no environmental threat; they are, in fact, useful commodities. In essence, a catalytic reductive detoxification route offers the attractive potential of a "waste-to-fuel" disposal route for these troublesome CW agents. The overall process is depicted in Figure 1.

There have been very few studies of combined hydrodesulfurization (HDS) and hydrodechlorination (HDC) to detoxify organic wastes [3-4], although HDS is a well-known hydrotreating process in the petroleum industry [5]. Bonnet et al. investigated HDS and HDC of halogenated benzothiophenes over a $CoO\text{-}MoO_3/Al_2O_3$ catalyst to study the effect from halogen groups [3]. Zhou et al. reported the first study of adsorption and thermal decomposition of CEES over Pt (111) surfaces [4]. A closely related investigation by Hagh and Allen reported the effect of H_2S on HDC of polychlorinated biphenyls (PCBs) over a presulfided Al_2O_3-supported Ni-Mo catalyst [6]. Although H_2S decreased the HDC reaction rate slightly, the results suggested that well-known HDS catalysts, such as Ni-Mo and Co-Mo, might be candidates for combined HDS and HDC of CEES. Another process developed by Kalnes and James of Universal Occidental Petroleum [7] demonstrated a pilot-scale hydrogenation of hazardous organic waste. Although both HDS and HDC reactions occurred during the process, no detailed information on the interaction between HDS and HDC was given.

Previously, we reported that 3% $Pt/\eta\text{-}Al_2O_3$ showed relatively higher activity and stability than other supported Pt catalysts for HDC of 1,1,1-trichloroethane [8]. In this study, we chose to investigate the activity and stability of 3% $Pt/\eta\text{-}Al_2O_3$ for catalytic hydrogenation of CEES. The presulfided Co-Mo and Ni-Mo catalysts work best at higher temperatures and pressures. However, with CW agents, a high-pressure reaction condition is not favorable because of the concern of producing highly noxious byproducts. This study investigates the combined HDC and HDS reactions of CEES and related compounds over supported Ni-, Co-, and Mo catalysts.

1.2 PLASMA TECHNOLOGY FOR SURFACE CLEANING

The U.S. Army has an urgent need to remove hazardous/explosive contaminants from structures, parts, and demiled artillery shells so they can be recovered, recycled, and reused. There are several hundred thousand tons of artillery shells in the United States alone that need to be decontaminated. Currently, the Army melts and recovers a majority of the explosive materials. The shell casings, however, contain grams of explosives depending on their sizes and shapes after the melting steps. The shell casings are subsequently cleaned to remove contaminants to a nonvisual level (3x level). Restrictions on transporting demiled shell casings mandate that the shell casing be cleaned to a 5x level. One possible method of cleaning the casings to this level is the hot-gas decontamination (HGD) process.

The HGD process was originally investigated by the U.S. Army Toxic and Hazardous Materials Agency (USATHAMA). Pilot studies have shown that decontamination of a structural component is possible using a heated gas to thermally decompose or volatilize explosives with subsequent incineration in an afterburner. As shown in Figure 2, parts and equipment are loaded in a flash chamber, which is heated with propane to vaporize the contaminants. The hot gas with vaporized contaminants is then oxidized by the afterburner to destroy the contaminants. Although the study results concluded that hot gas is effective in removing most explosives and propellant compounds, the following disadvantages of the HGD process were identified:

- Long cycle time: The HGD process requires extended time to heat up and cool down the reaction chamber. The decontamination cycle could be as long as several days depending on the reaction temperature and how long the chamber has to remain at steady state to vaporize the explosives.
- Not adequate for nonmetal parts: The HGD process is not adequate to treat aluminum or nonsteel parts such as clay. They crack and become brittle and thus are easily broken after exposure to the hot gas.
- Not successful for intricate components: Structures containing intricate or mechanical components were not successfully treated with the HGD process and could not be reused.
- Large volume of exhaust emissions: The HGD process generates a large volume of flue gas that may require treatment before being released into the air. For example, NO_x is produced from the direct oxidation of nitrogen atoms in the compounds. Also, the gas mixture from the flash chamber is oxidized in a thermal oxidizer or an afterburner at a temperature above 1,000 °C, which will generate some prompt NO_x on its own. NO_x emissions must meet U.S. Environmental Protection Agency (EPA) regulations before being released.

These disadvantages have prompted the investigation of alternative cleaning methods to achieve the 5x level that are less expensive, less destructive, and reduce overall cleaning time.

A radio frequency (RF) nonthermal plasma technique was proposed to remove the energetic materials to a level that allows the shells to be reused while maintaining the integrity of the materials. RF plasma, as demonstrated in our previous reports, can selectively remove the explosive layer on top of the paint coating of the shell. Its delicate control of surface

contaminant removal is surprisingly efficient, and the process can be completed within a few minutes, depending on the power, cycle, and plasma type used. Compared to the HGD process, RF plasma technology can economically, effectively, and efficiently remove the contaminants without sacrificing the integrity of the materials treated. Table 1 compares RF plasma technology with the HGD process. RF technology has the following cost, environmental, and performance advantages:

- Reduced cost: The operating cost is estimated to be less than $30 per metric ton of shell casings, about half of the operating cost of the HGD process. The nonthermal plasma process operates at room temperature, so no additional fuel is required to heat gases.

- Environmentally friendly: The process uses only electricity and is therefore environmentally clean. The nonthermal plasma process requires only 5 to 10 mL/min of flow while the exhaust gas of the HGD process is ~ 2,000 ft^3/min. NO_x emissions from any decontamination processes will be regulated by EPA. High-temperature combustion in the HGD process generates thermal NO_x (oxidation of nitrogen in air) as well as fuel NO_x from explosives (oxidation of nitrogen in explosives). Fuel NO_x can be reduced and controlled by the nonthermal plasma process.

- Strong performance: The nonthermal plasma system has been demonstrated to destroy up to 99.98% of 1.0 g TNT on an 81-mm shell with a one-step treatment. The cycle time for treatment could be as low as 10 to 15 minutes. This short treatment cycle time minimizes the impact of failed treatments on overall process efficiency. It is much more flexible economically and in terms of scheduling. HGD, on the other hand, requires two treatment steps—vaporization and combustion. Its destruction removal efficiency can be as high as 99.999% for most steel components, but the process is not effective for nonsteel or intricate parts. The cycle time for the HGD process ranges from 1 to 2 days. If any test fails, the whole batch is rejected, thus wasting 1 to 2 days of effort. The materials treated by the nonthermal plasma process will likely be maintained for recovery, recycle, and reuse because they will not be exposed to high temperatures as in the HGD process.

Table 1. Cost, Environmental, and Performance Advantages of Nonthermal Plasma Process Over HGD Process

		Nonthermal Plasma	HGD
Cost	Operating	<$30.00/metric ton	$60.87/metric ton
	Fuel requirement	No	Yes
Environmental	Exhaust emission	<0.004 ft^3/min	~2,000 ft^3/min
	Fuel NO_x	Yes, but reduced	Yes
	Thermal NO_x	No	Yes
Performance	Cycle time	<1 h	24-60 h
	Nonmetal and intricate parts	Yes	No
	Temperature shells exposed to	Low (<100 °C)	High (260-370 °C)

2.0 RESULTS AND DISCUSSION

2.1 HYDROTREATMENT OF CHEMICAL WASTES

2.1.1 Hydrotreatment of Chloroethyl Ethyl Sulfide (CEES)

We have systematically tested 3% Pt/η-Al_2O_3, Ni/AC, Mo/AC, Ni-Mo/AC, Ni-Mo/γ-Al_2O_3, and Co-Mo/γ-Al_2O_3 catalysts for hydrotreatment of CEES as a simulant for HD. Results showed complete conversion was obtained over 3% Pt/η-Al_2O_3, Ni-Mo/γ-Al_2O_3, Co-Mo/γ-Al_2O_3, Mo/AC, and Ni-Mo/AC at 300 °C with a 30:1 ratio of H_2/CEES. The overall activity and stability order for these catalysts is Ni-Mo/AC ≈ Ni-Mo/γ-Al_2O_3 > Co-Mo/γ-Al_2O_3 > 3% Pt/η-Al_2O_3 ≈ Mo/AC > Ni/AC. Thermodynamic calculation of the reaction; the effect of reaction variables on activity, selectivity, and stability; and possible reaction pathways are summarized and discussed in the following sections.

2.1.1.1 3% Pt/η-Al_2O_3

The conversion of CEES and product distribution versus temperature were tested at temperatures ranging from 170 to 300 °C, with 200 cm^3/min of 1% CEES, 25% H_2, and the balance helium. The results, summarized in Figure 3, show that the overall conversion of CEES increases with temperature. Approximately 20% CEES is converted at 170°C, and the conversion is complete above 230 °C. The product distribution, however, is more complex. As shown in Equation 1, possible HDC products, such as diethyl sulfide, ethene, and ethane, and possible HDS products, such as chloroethane, methyl mercaptan, ethene, and ethane, were detected. The results suggest that both HDC and HDS reactions proceed in parallel during the hydrogenation of CEES. The selectivities to both diethyl sulfide and chloroethane decrease with increasing temperature while hydrocarbon selectivity increases. On the other hand, the selectivity to ethyl mercaptan goes through a maximum at a temperature between 200 and 230 °C. These results suggest ethyl mercaptan may not be a simple product from HDC of CEES. (It is also possible that ethyl mercaptan can be formed from the hydrogenation of diethyl sulfide, which is not shown in Equation 1 [9].) Because the concentration of chlorinated hydrocarbons (i.e., chloroethane) is much less than the total concentration of sulfur-containing products (ethyl mercaptan and diethyl sulfide) at all temperatures tested, it appears that total HDC of CEES is faster than HDS of CEES over 3% Pt/η-Al_2O_3.

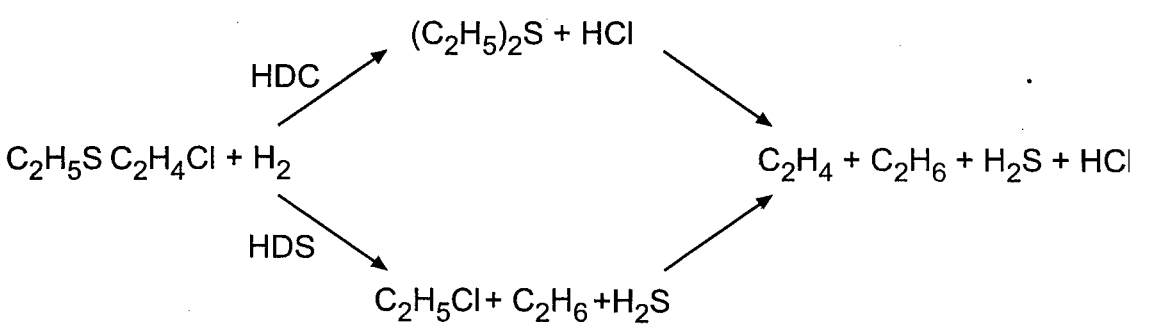

(1)

Figure 4 shows the long-term stability of 3% Pt/η-Al_2O_3 for the hydrogenation of CEES at 250 °C. The hydrogenation activity is stable during the 20-h run with ~100% CEES conversion.

The major products are ethene and ethane (~80% selectivity to these two products), with ~20% of the product going to ethyl mercaptan and diethyl sulfide. The selectivities to both hydrocarbon and sulfur-containing products remain constant during the run. This result suggests that H_2S and HCl, the HDS and HDC reaction products, have no apparent effect on the stability and selectivity of hydrogenation of CEES over 3% Pt/η-Al_2O_3. This result is similar to that of Hagh and Allen who showed that H_2S does not affect the lifetime of the catalyst for HDC of PCBs on various catalysts [6]. (Because the chloroethane concentration is <100 ppm throughout the run, it is not included in Figure 4.) This suggests, again, that the total HDC reaction is faster than total HDS for the hydrogenation of CEES over 3% Pt/η-Al_2O_3.

2.1.1.2 Ni-Mo/γ-Al_2O_3 and Co-Mo/γ-Al_2O_3

The conversions and hydrocarbon selectivity of hydrotreating CEES over γ-Al_2O_3-supported Ni-Mo and Co-Mo catalysts were studied at both 250 and 300 °C with 200 cm^3/min of 0.33% CEES, 10% H_2, and the balance helium. At 300 °C, both the Ni-Mo and Co-Mo catalysts were active and stable for 20 h for HDS and HDC of CEES. As shown in Figure 5, Ni-Mo showed no sign of deactivation, with 98% selectivity to ethylene and ethane throughout the 100-h run. However, Co-Mo was slightly less active than Ni-Mo, as indicated by the slow decrease of hydrocarbon selectivity during the first 20 h of the run.

The superior activity and stability of Ni-Mo over Co-Mo is more obvious at 250 °C. As shown in Figure 6, the HC selectivity of Co-Mo decreases from ~88% to ~47%, but the HC selectivity of Ni-Mo decreases only slowly from 95% to 90%.

2.1.1.3 Ni/AC, Mo/AC, and Ni-Mo/AC

The conversions and hydrocarbon selectivity of hydrotreating CEES were studied at temperatures from 200 to 300 °C over Ni-Mo, Mo, and Ni catalysts supported on active carbon (AC). At 300 °C, Ni-Mo/AC is the most active and stable catalyst for HDS and HDC of CEES. The HC selectivity over Ni-Mo/AC is >99.5%, higher than the 98.0% hydrocarbon selectivity over Ni-Mo/Al_2O_3, as shown in Table 2. This suggests that AC-supported Ni-Mo catalysts will be more effective for hydrotreating mustard gas with fewer byproducts.

Table 2. Comparison of Activity and Selectivity for Hydrotreating CEES Over Various Catalysts

Catalysts	CEES Conversion* (%)	HC Selectivity (%)
Ni-Mo/AC	100.0	>99.5
Mo/AC	100.0	94.0
Ni/AC	51.1	<20.0
Ni-Mo/Al_2O_3	100.0	98.0

Note: Test conditions = 300 °C after 20 h on stream.

Neither Mo/AC nor Ni/AC was as active or as stable as Ni-Mo/AC for hydrotreating CEES. As shown in Table 2, the HC selectivities over Mo/AC and Ni/AC are lower than the selectivities over Ni-Mo/AC and Ni-Mo/Al_2O_3 (94.0% and <20%, respectively). The HC production distributions are similar for all the catalysts tested except Ni/AC, with ethylene being the major product (~80%) and ethane the minor product (~20%). In the case of Ni/AC, no ethane was

formed during the hydrotreatment of CEES. Sulfur deactivates Ni, which is evidenced by the negligible formation of ethane and lowest CEES conversion, with 51.1% after 20 h on stream.

2.1.2 *Hydrotreatment of Diethyl Sulfide (DES) and Chloroethane (CE)*

DES and CE are possible intermediates of HDS and HDC of CEES, respectively. DES is produced by the removal of the one chlorine atom in CEES and the hydrogenation of the bond. CE is produced by the hydrogenolysis of the C-S bond in CEES. HDS of DES was studied over Ni-Mo/AC, Mo/AC, Ni/AC, and Ni-Mo/-Al_2O_3 at 300 °C; 1.8% DES, 10% H_2, and the balance He; and a space velocity of 120,000 $cm^3/h/g•cat$. The HDS activities were measured after 20 h on stream. Table 3 summarizes the DES conversions, hydrocarbon selectivities, and C_2H_6/C_2H_4 ratios over AC-supported Ni, Mo, Ni-Mo catalysts and the Ni-Mo/-Al_2O_3 catalyst. Ni-Mo/AC and Ni-Mo/-Al_2O_3 catalysts have similar activity (54.7% and 58.4%) and selectivity (73.9% and 78.2%) for HDS of DES. However, both Mo/AC and Ni/AC have much lower activity than supported Ni-Mo catalysts with 11.6% and 17.1% DES conversion, respectively. On the other hand, the C_2H_6/C_2H_4 ratios in the product stream are similar for Ni-Mo/AC (0.19) and Ni-Mo/-Al_2O_3 (0.16), but are very different for Mo/AC and Ni/AC. The results indicate that Mo/AC is more selective to C_2H_6 than either supported Ni-Mo catalysts or Ni/AC. The C_2H_6/C_2H_4 ratio resulting from the Mo/AC catalysts is 0.43, compared to 0.16 to 0.19 for the supported Ni-Mo catalysts. Ni/AC is not active for hydrogenation at all, with a C_2H_6/C_2H_4 ratio of 0, as shown in Tables 3 and 4.

Table 3. Comparison of Conversion and Selectivity for Hydrotreating Diethyl Sulfide

Catalysts	DES Conversion (%)	HC Selectivity (%)	C_2H_6/C_2H_4 Ratio
Ni-Mo/γ-Al2 O_3	58.4	78.2	0.16
Ni-Mo/AC	54.7	73.9	0.19
Mo/AC	11.6	65.2	0.43
Ni/AC	17.1	73.0	0.0

Note: Test Conditions = 1.8%, 10% H_2, and balance He; 300 °C; 200 cm^3/min; 0.1 g of catalysts.

Table 4. Comparison of Hydrotreating and Selectivity for Hydrotreating CEES

Catalysts	CEES Conversion (%)	HC Selectivity (%)	C_2H_6/C_2H_4 Ratio
Ni-Mo/AC	100	>99.5	0.25
Mo/AC	100	94.0	0.30
Ni/AC	51.1	<20	0.0
Ni-Mo/Al2O3	100	98.0	0.28

Note: Test conditions = 0.33% CEES, 10% H_2, and balance He; 200 cm^3/min; 0.5 g of catalysts; 300 °C after 20 h on stream.

HDC of CE was also studied over the same group of catalysts at 300 °C; 1.2% CE, 10% H_2 (balance He) at 120,000 $cm^3/h/g{\cdot}cat$ were used over 0.1 g of catalysts. The results are summarized in Table 5. All catalysts were treated with 10% H_2S/H_2 at 400°C for 1.5 h, as were all catalysts used in other HDS or HDS+HDC reactions. As shown in Table 5, all catalysts showed measurable conversion of CE to ethane and HCl, although Ni/AC is clearly less active for this reaction. Both Ni-Mo/AC and Ni-AC showed negligible hydrogenation activity during HDC of CE, forming only ethylene. Although Mo/AC has good hydrogenation activity during hydrotreatment of CE with a C_2H_6/C_2H_4 ratio of 0.20, it is less active for CE conversion than supported Ni-Mo catalysts.

The stoichiometric reaction of CEES to ethylene (Equation 2) requires only a 1:1 ratio of H_2: CEES, although a 3:1 ratio of H_2: CEES is required to produce ethane (Equation 3).

$$C_2H_5 - S - C_2H_4Cl + H_2 \rightarrow 2C_2H_4 + HCl + H_2S \quad (2)$$

$$C_2H_5 - S - C_2H_4Cl + 3H_2 \rightarrow 2C_2H_6 + HCl + H_2S. \quad (3)$$

Table 5. Comparison of Activities for Hydrotreating Chloroethane

Catalysts	CE Conversion (%)	C_2H_6/C_2H_4 Ratio
Ni-Mo/-Al_2O_3	61.2	0.03
Ni-Mo/AC	32.5	<0.01
Mo/AC	20.6	0.20
Ni/AC	3.5	0.0

Note: Test conditions = 1.2%, 10% H_2, and balance He; 300 °C; 200 cm^3/min; 0.1 g of catalysts.

As shown in Equations 2 and 3, HDS and HDC of CEES can potentially produce C_2H_6 or C_2H_4 as final products as well as HCl and H_2S, depending on the H_2:CEES ratio. Thermodynamic calculations, shown in Figure 7, suggest that C_2H_6 is the most stable product at 250 °C when the H_2:CEES ratio is equal to or larger than 3:1. Although other products, such as ethylene, DES, and ethyl mercaptan, are stable when the H_2:CEES ratio is less than 3:1, they are not thermodynamically favored when the H_2:CEES ratio is ≥3:1. Experimentally, sulfur-containing components are detected in the product stream even with an H_2:CEES ratio of 30:1 at 300 °C over supported Ni and/or Mo catalysts.

2.1.2.1 Reaction Pathways

The possible reaction pathways, as shown in Equation 1, indicate that the HDS+HDC of CEES could be either HDC followed by HDS or HDS followed by HDC. DES would be a reaction intermediate if the HDC reaction comes first. On the other hand, CE would be a reaction intermediate if HDS precedes the HDC reaction.

Based on the results shown in Table 4, Ni-Mo/γ-Al_2O_3, Ni-Mo/AC, and Mo/AC (except Ni/AC) have similar CEES conversion, hydrocarbon selectivity, and C_2H_6/C_2H_4 ratio in the product stream during hydrotreatment of CEES. This suggests that the hydrotreatment of CEES goes through similar reaction pathways over these catalysts. By examining the results in Table 3, the activity of HDS of DES shows similar hydrocarbon selectivity for all four catalysts, but the DES conversion is much higher for supported Ni-Mo catalysts than Mo/AC or Ni/AC. Furthermore, the C_2H_6/C_2H_4 ratio for Mo/AC is much higher than for both Ni-Mo/AC and Ni-Mo/γ-Al_2O_3, which indicates that supported Ni-Mo catalysts are very active for breaking the C-S bonds, but not as active as Mo/AC for hydrogenation of C_2H_4 to C_2H_6 during HDS of DES. These results suggest that hydrotreating CEES to C_2H_6 and C_2H_4 is not likely to follow the same reaction pathways as HDS of DES.

The CE reaction activity and selectivity over these four catalysts, as summarized in Table 5, show different conversions. There is no similarity between any two catalysts for conversion of CE. However, both supported Ni-Mo catalysts and Ni/AC show negligible hydrogenation activity during HDC of CE. The results indicate HCl inhibits the hydrogenation activity of catalysts but does not significantly influence Mo/AC. This suggests C_2H_6 formed during the hydrotreatment of CEES over supported Ni-Mo catalysts does not come from HDC of CE. It also suggests that CE is not likely an intermediate during the hydrotreatment of CEES. This speculation is further supported by the fact that we have detected negligible CE concentrations throughout the hydrotreatment reactions of CEES.

The activity orders of these catalysts for conversion of CEES, DES, and CE and their C_2H_6/C_2H_4 ratio in the product stream are summarized in Table 6. The orders for activity and C_2H_6/C_2H_4 production ratio for hydrotreating CEES are very different from HDS of DES or HDC of CE. The results suggest that hydrotreatment of CEES is not dominated by HDS of DES, HDC of CE, or a combination. In fact, we have detected two sulfur-containing compounds, 1,4-dithiane ($C_4H_8S_2$) and 1,2-bis (ethylthio) ethane (C_2H_5-S-C_2H_4-S-C_2H_5), in the product stream at low residence times. We speculate that the S-C_2H_5Cl bond, due to the weakening effect from Cl, will be broken first to form C_2H_5-S* and *C_2H_4Cl intermediates (Equation 4). In fact, Zhou et al. reported that CEES dissociation begins with cleavage of the S-C bond on the chlorine side (C_2H_5S-CH_2CH_2Cl) when multi-layers of CEES are present on Pt surface [4]. It is likely that C_2H_5S* can react with another CEES molecule to form 1,2-bis (ethylthio) ethane, then 1,4-dithiane is formed by cyclization and release of a C_2H_6 molecule (Equations 5 and 6).

Table 6. Activity Summary for Hydrotreatment of CEES, DES, and CE

Hydrotreatment	Conversion Activity	C_2H_6/C_2H_4 Ratio
CEES	Ni-Mo/AC ~ Ni-Mo/Al_2O_3 ~ Mo/AC >> Ni/AC	Mo/AC ~ Ni-Mo/Al_2O_3 ~ Ni-Mo/AC >> Ni/AC
DES	Ni-Mo/Al_2O_3 ≈ Ni-Mo/AC >>Ni/AC>Mo/AC	MO/AC > Ni-Mo/AC ≈ Ni-Mo/Al_2O_3 >> Ni/AC
CE	Ni-Mo/Al_2O_3 > Ni-Mo/AC > Mo/AC >> Ni/AC	Mo/AC > Ni-Mo/Al_2O_3 ≈ Ni-Mo/AC ≈ Ni/AC

$$C_2H_5S - C_2H_4Cl + 2^* \longrightarrow C_2H_5S^* + {}^*C_2H_4Cl \quad (4)$$

$$C_2H_5S^* + C_2H_5 - S - C_2H_4Cl \longrightarrow C_2H_5 - S - C_2H_4 - S - C_2H_5 + {}^*Cl \quad (5)$$

$$C_2H_5 - S - C_2H_4 - S - C_2H_5 \longrightarrow \text{(S-ring)} + C_2H_6 \quad (6)$$

2.1.2.2 Destruction Efficiency Determination with FPD

Because the detection limit of the previous mass selective detector (MSD) is ~10 ppm, we can only conclude that the best destruction efficiency of CEES is >99.9% over Ni-Mo/AC, although no CEES is found in the effluent. It is essential to improve the detector sensitivity to determine if the destruction efficiency could be as high as 99.999% or even higher. The detection limit of the FPD system we use is about 100 ppb. As mentioned in the previous section, the conversion activity of Ni-Mo/Al_2O_3 is comparable to the activity of Ni-Mo/AC, but the byproduct selectivity is lower over Ni-Mo/Al_2O_3 than over Ni-Mo/AC.

Figure 8 shows the results of testing 2% CEES, balance H_2, and total flow of 50 cm^3/min over 0.5 g of Ni-Mo/AC catalysts at 300 °C. The CEES concentration in the effluent was down to ~9 ppm within 30 min, corresponding to 99.955% destruction efficiency. The concentration of CEES decreased further with time on stream as shown in Figure 8. After 12 h on stream, the effluent CEES concentration stabilized at ~800 ppb, which corresponds to a DRE of 99.996%. The reaction takes ~12 h to reach the maximum destruction activity, which suggests that, the catalytic surface is continuously modified during the reaction. Hydrotreatment of CEES generates H_2S by removing sulfur from CEES by H_2, and we suspect that longer H_2S/H_2 pretreatment may decrease the time required to reach the maximum activity. However, we pretreated Ni-Mo/AC under 10% H_2S/H_2 at 400 °C overnight instead of over 2 h and no improvement on destruction efficiency for CEES conversion was found. Changing the reaction temperature did not improve the destruction efficiency either. However, when we tested an MZ391-supported Pt catalyst, a DRE of 99.998% was achieved at 350 °C, but ~20 h was needed to reach maximum activity.

2.2 Plasma Technology for Surface Cleaning

After the successful tests of explosive samples with the RF plasma treatments, we successfully designed and set up an RF plasma system for full-size shell tests at RTI. Results were presented at the 1999 and 2000 Strategic Environmental Research & Development Program (SERDP) Symposium and Workshop. The plasma system, shown in Figures 9 and 10, consists of electronic devices for power supply, a reaction chamber to hold shell casings (e.g., 81 mm), and a gas delivery system for controlled flow of various plasma sources. Both the chamber walls (6-in diameter) and the 3/8-in stainless tube for gas delivery in the middle of the reaction chamber are grounded. A quartz window on the side is for viewing and spectra emission detection. The full-size shell plasma system is designed to clean both the inside and outside

surfaces of shell casings. It can operate under continuous or pulse modes (nanoseconds to seconds).

Figure 11 shows the top view of the plasma chamber when plasma is lighted up at continuous mode. Plasma intensity looks uniform throughout the chamber. Up to 800 W of power output can be provided by the EIN A-500 amplifier to the plasma reactor. The decontamination of DNT, TNT, RDX, and Comp B using the full-size system is summarized in the following sections.

2.2.1 Decontamination of Dinitrotoluene (DNT)

2.2.1.1 Direct Cleaning Analysis with Nitrogen Phosphorus Detector

Comparison of O_2, H_2, and H_2O Plasmas. Preliminary cleaning tests of DNT on different shell surface locations were carried out with the nitrogen phosphorus detector (NPD) to determine the cleaning efficiency of plasma on various shell surfaces. It is expected that different shell surface locations will have different cleaning efficiencies because plasma intensities are somewhat different due to the various distances between electrodes (shell body) and the grounds (chamber walls and the inside gas delivery tube). Silicon carbide samplers (Nicolet) with 1-cm diameters (~0.8-cm^2 area) were loaded with 10 to 15 mg of DNT and stuck to four representative locations of shell wall surfaces—the inside middle, inside bottom, outside top, and outside middle. Continuous plasmas of 200 W, including O_2, H_2, and H_2O, were tested for 25 min. After the plasma cleaning, samples were peeled off and kept in vials with 1.0 mL of toluene overnight. The resulting solutions were then analyzed by GC with an NPD to determine the amount of DNT left after the plasma treatments. Table 7 summarizes the results, including sample loadings, DNT residue after treatment, and calculated DRE. The DRE ranges from 97 to 99.9% with 200 W power for 25 min of treatment using different plasma gases. The results suggest that the three plasmas tested (O_2, H_2, and H_2O) have similar cleaning effects for DNT, but H_2 plasma appears to be more uniform throughout the plasma chamber according to the more uniform DRE of four different sample locations under H_2 plasma. Although the DREs are not extremely high, it is important to compare different plasmas under conditions with measurable DRE differences.

Systemic Study of H_2 Plasma for Decontamination of DNT. Because the preliminary tests of DNT decontamination indicate that H_2 plasma is the more uniform and effective plasma to decompose DNT, our further investigations focus on H_2 plasma with different parameters such as treatment time, pressure, on/off duty cycle, and power. We tested only the surface at the outside middle location because it is the most difficult place to clean according to the results reported in the previous section. The total flow of hydrogen is maintained at 5 mL/min.

Effect of Treatment Time. As listed in Table 8, the length of treatment time affects the DRE tremendously in the beginning. For example, the DRE increases from 56.2% to 94.5% when treatment time increases from 12 to 21 min. In addition, the DRE increases from 94.5% to 99.46% when the treatment time increases from 21 to 25 min. However, further increase of the treatment time does not improve the DRE effectively. By visual inspection of the samples after the plasma treatment, we found the explosive sample formed a protective layer on the top, which we suspect is a polymer film derived from DNT. It may be difficult for the plasma to

penetrate and clean the residual DNT at the bottom closer to the sample surface. Further investigation focused on minimizing the protective layer formation and improving the DRE.

Table 7. Cleaning Efficiency of Various Plasmas for DNT on Four Representative Locations

Plasma Gas	Sample Locations	DNT Loading (mg)	DNT Residue (μg)	DRE (%)
O_2	Inside middle	11.0	100.4	99.08
	Inside bottom	13.7	12.0	99.91
	Outside top	17.0	328.0	98.07
	Outside middle	15.4	397.3	97.42
H_2	Inside middle	10.0	33.0	99.67
	Inside bottom	10.8	15.4	99.86
	Outside top	13.0	98.9	99.24
	Outside middle	12.0	109.2	99.09
H_2O	Inside middle	15.8	86.2	99.45
	Inside bottom	15.4	16.6	99.89
	Outside top	12.6	144.8	98.85
	Outside middle	10.2	294.6	97.11

Note: Test conditions = 500 mtorr, 5-mL/min flow at 200 W for 25 min.

Table 8. Effect of Treatment Time on DRE

Treatment Time (min)	DNT Loading (mg)	DNT Residue (μg)	DRE (%)
12	41.6	18,219	56.2
21	72.0	3,959	94.5
25	39.1	209.2	99.46

Note: Test conditions = 500 mtorr, 200 W, 25 min.

Effect of On/Off Duty Cycle. Using milder conditions to avoid polymerization precursors seems to be a reasonable approach to achieve higher DRE yet still minimizes the protective layer formation during H_2 plasma treatment. We tested three different duty cycles with a longer treatment time of 56 min. Treatment time is an important economical factor in scaling up the process and is discussed in Section 2.2.5. As shown in Table 9, we tested three on/off duty cycles—0.3 ms/0.6 ms, 3 ms/6 ms, and 30 ms/60 ms—at 200 W and 500 mtorr total pressure. Although the total power outputs of the three tests are the same, the results are different: the 3 ms/6 ms cycle is the most effective, with 99.71% DRE, followed by the 30 ms/60 ms cycle, with 99.24% DRE. The 0.3 ms/0.6 ms cycle is the least efficient, with 93.8% DRE. We do not know why these three cycles showed different DREs, but we suspect it depends on the lifetime of various intermediates during the treatment process.

Table 9. Effect of On/Off Duty Cycle on DRE

On/Off Cycle	DNT Loading (mg)	DNT Residue (μg)	DRE (%)
0.3 ms/0.6 ms	37.8	2,343.0	93.80
3 ms/6 ms	38.9	111.2	99.71
30 ms/60 ms	39.4	299.0	99.24

Note: Test conditions = 500 mtorr, 200 W, 56 min.

Effect of Plasma Pressure. As discussed, we found that the on/off cycle in the millisecond range seems to be more efficient than other on/off cycles. According to the literature [10], the pressure of the plasma system affects the plasma generation and ion and radical distributions tremendously. There are more gas molecules available to be excited or ionized by high-energy electrons under high-pressure conditions. However, ions and radicals are short-lived because they have more chances to collide with other molecules and lose their energy.

As shown in Table 10, we investigated the effect of pressure ranging from 200 to 900 mtorr on DRE at 200 W, a 3 ms/6 ms duty cycle, and a total treatment time of 56 min. The sample loadings of DNT are similar (38 to 40 mg). The DRE order is 200 mtorr ≈ 300 mtorr > 500 mtorr >>700 mtorr >>900 mtorr. These results suggest that lower pressure favors higher DRE under our testing conditions. Although the calculated DRE with total pressure of 200 mtorr is slightly higher than the DRE with 300 mtorr, we considered the efficiencies at 200 mtorr and 300 mtorr to be the same within the experimental error. Therefore, we continued to investigate the plasma treatment process at a total pressure of 300 mtorr.

Table 10. Effect of Plasma Pressure on DRE

P (mtorr)	DNT Loading (mg)	DNT Residue (μg)	DRE (%)
200	39.7	85.0	99.79
300	38.7	94.6	99.76
500	38.9	111.2	99.71
700	39.7	1,062.0	97.32
900	40.5	1,237.0	96.94

Note: Test conditions = 3 ms/6 ms, 200 W, 56 min.

Effect of Power and Duty Cycle Combination. We further lowered the power of the plasma system to 300 mtorr to achieve higher DREs. Table 11 lists DREs at various combinations of power and duty cycles. Except for the DRE of 88.48% at 100 W and 4.5 ms/4.5 ms duty cycle, all other DREs were higher than 99% after 56 min of treatment. The best three conditions were 100 W with a 6 ms/3 ms cycle, 75 W with continuous wave, and 200 W with a 3 ms/6 ms cycle, with DREs of 99.86%, 99.76%, and 99.76%, respectively. To ensure that H_2 plasma is more efficient than O_2 plasma for DNT destruction, we again compared H_2 plasma and O_2 plasma under 200 W, 3 ms/6 ms conditions and under 100 W, continuous wave conditions. Higher DREs at both conditions with H_2 plasma, as listed in Table 12, confirm that H_2 plasma is more efficient for DNT destruction than O_2 plasma.

Table 11. DREs at Various Power and Duty Cycle Combinations

Power (W)	Duty Cycle	DNT Loading (mg)	DNT Residue (μg)	DRE (%)
200	3 ms/6 ms	38.7	94.6	99.76
100	4.5 ms/4.5 ms	38.2	4,402.0	88.48
100	CW	38.1	118.4	99.69
100	6 ms/3 ms	38.8	55.7	99.86
75	CW	39.7	95.9	99.76
200	6 ms/3 ms	40.6	170.0	99.58
200	4.5 ms/4.5 ms	38.8	350.5	99.10

Note: Test conditions = 300 mtorr, 56 min.

Table 12. Comparison of H_2 Plasma and O_2 Plasma

Plasma Type	Power/Duty Cycle	DNT Loading (mg)	DNT Residue (μg)	DRE (%)
H_2	200 W, 3 ms/6 ms	38.7	94.6	99.76
O_2	200 W, 3 ms/6 ms	39.2	617.0	98.43
H_2	100 W, CW	38.1	118.4	99.69
O_2	100 W, CW	39.2	615.5	98.43

Note: Test conditions = 300 mtorr, 56 min.

2.2.1.2 On-line Mass Spectrometry Analysis

As shown in Table 11, both pulsed and continuous wave plasmas can effectively decontaminate the explosive stimulant, DNT, on shell surfaces. To understand the product formation resulting from the plasma cleaning and the cleaning reaction mechanism, we installed a mass spectrometer downstream to analyze the products during the decontamination process. The tests monitored were H_2 plasmas with on/off duty cycles of 0.3 ms/ 0.6 ms, 3 ms/6 ms, and 30 ms/60 ms at 200 W and a total pressure of 500 mtorr. The results are summarized in Figures 12 through 17. As shown in Equations 7 and 8, possible products from DNT decomposition and DNT reaction with hydrogen plasma include hydrocarbons, carbon monoxide, carbon dioxide, water, nitrogen, nitrous oxide, and nitrogen oxides. DNT was also monitored to determine if any unreacted gaseous DNT slipped through without reacting with plasma. The only hydrocarbon products monitored were methane, ethane, benzene, and toluene. There was some small amount of methane detected, but negligible benzene and toluene. Therefore, we focused our investigation on the rest of the possible products.

$$C_7H_6N_2O_4 \rightarrow C_xH_y + CO + CO_2 + H_2O + N_2 + N_2O + NO_x \quad (7)$$

$$C_7H_6N_2O_4 + H \rightarrow C_xH_y + CO + CO_2 + H_2O + N_2 + N_2O + NO \quad (8)$$

N_2, CO_x, N_2O, and H_2O. As shown in Figures 12, 13, and 14, the abundance of various mass numbers (28, 44, and 18) of all three tests increased abruptly when the plasma was initiated.

The abundances settled down to a steady level followed by a large peak at around 50 min, then returned to a somewhat lower level than the steady level before the maximum peak. When the plasma was stopped, the abundances dropped quickly. The abundance level after the peak was lower than the level before the peak, suggesting that there are reactions between plasma and DNT at solid state before the large peak, but with slow rates. The maximum peaks, at ~50 min, indicate that there are vigorous reactions between DNT and plasma and that various products are formed. The timing of the maximum peak is coincident with the melting (and maybe vaporization) of the DNT (visual inspection through the quartz window), which suggests that the reaction of liquid or gaseous phases of DNT is much faster than the solid phase. The melting (and vaporization) of DNT results from the slow heating of the shell due to the heat generated from the electron/ions bombarding the surfaces and the internal resistance of the shell when high voltage is applied. All three spectra in Figures 12, 13, and 14 show apparent peaks for mass numbers 28, 44, and 18. We are confident that detection of mass number 18 is due to the formation of H_2O in the process. But detection of mass number 28 could be due to the formation of either N_2 or CO, and detection of mass number 44 could be due to the formation of CO_2 or N_2O. Another trap technique using liquid nitrogen to liquify the products downstream of the plasma treatment process was investigated. The trapped products were isolated and heated up to vaporize the condensed products after the plasma treatment. Then gas samples were taken with an airtight syringe for GC analysis. Results showed no sign of CO or N_2O in the trapped products, which confirms that mass number 28 is N_2 and mass number 44 is CO_2. These results indicate that the major products from H_2 plasma cleaning of DNT are N_2, CO_2, and H_2O, which are environmentally benign.

NO NO_2 and, DNT. We also monitored NO (#30), NO_2 (#46), and the vaporized and unreacted DNT (#165) during the plasma treatment. The results are shown in Figures 15, 16, and 17. NO abundance in tests with 0.3 ms/0.6 ms (Figure 15) and 3 ms/6 ms (Figure 16) increased from the initiation of the plasma, which confirms that the plasma does react with solid-phase DNT as mentioned earlier. The relatively small peaks at ~50 min, matching the peak positions of N_2, CO_2, and H_2O, also suggest that the majority of NO is formed during the vigorous reaction of plasma and DNT, but it is a minor product compared with large N_2, CO_2, and H_2O peaks. The test with a duty cycle of 30 ms/60 ms, as shown in Figure 17, was quite different from the tests with duty cycles of 0.3 ms/0.6 ms and 3 ms/6 ms. NO abundance increased only slowly with time, but showed a much bigger peak at ~50 min. These results suggest the plasma reaction with solid DNT is much slower with the 30 ms/60 ms duty cycle, and the major cleaning reaction is completed when DNT turns to liquid or vapor. The difference between the 30 ms/60 ms duty cycle and 0.3 ms/0.6 ms and 3 ms/6 ms duty cycles for the release of NO may be related to the type and the lifetime of the excited states of DNT when it is struck by the radicals/ions from different pulsed plasmas.

NO_2 abundance trends are also shown in Figures 15, 16, and 17. All three tests have similar NO_2 trends, but with much smaller abundance than NO. The results suggest the major component in NO_x is NO. We do not have quantitative measurements, but the ratio of NO to NO_2 is estimated to be about 10:1 to 15:1 based on the area under the curves.

There is no indication of unreacted DNT bypassing the plasma treatment during the treatment processes as shown in Figures 15, 16, and 17. We have successfully demonstrated that the

low-pressure RF plasma process is very efficient and environmentally friendly for cleaning the surfaces of artillery shell casings. Although there is NO_x in the product stream, the quantity is minor. The major decontamination products are N_2, CO_2, and H_2O.

2.2.1.3 Light Emission Monitoring with UV Spectrometer

Figures 18, 19, and 20 show the emission spectra of DNT with H_2O, H_2, and O_2 plasmas, respectively. The spectra of all tests are similar. The intensity increases through a maximum then decreases to a level close to the initial intensity. The maximum indicates a strong interaction between plasmas and DNT. Although the peak positions are similar among all three plasmas with three major peaks at 482.4 nm, 517.5 nm, and 559.6 nm, peaks that change most dramatically can be used most effectively to monitor the decontamination reactions. Selected major emission peaks are 387.5 nm and 656.7 nm for H_2 plasma; 336.5 nm, 355.9 nm, and 606.8 nm for H_2O plasma; and 336.5 nm and 355.9 nm for O_2 plasma with our system. The time needed to decontaminate most DNT depends on the plasma gases, the power wattage, and the pulse duty cycle. As shown in Figure 18, H_2O plasma at 200 W and a 0.3 ms/0.6 ms duty cycle can decontaminate DNT within 12 minutes. H_2 plasma (100 W, CW) and O_2 plasma (200 W and 3 ms/6 ms duty cycle) require ~45 minutes and ~50 minutes, respectively, to decontaminate DNT, as shown in Figures 19 and 20.

Selected peaks can be monitored for decontamination continuously during the process. One example is shown in Figure 21. Five peaks at 312 nm, 387 nm, 430 nm, 519 nm, and 656 nm were monitored throughout the process of decontaminating TNT with H_2 plasma. This example demonstrates that the UV emission spectrometer is an excellent and economical tool to monitor the progress of the plasma decontamination process and to determine the decontamination endpoint.

2.2.2 Decontamination of Trinitrotoluene (TNT)

2.2.2.1 Direct Decontamination Analysis with GC/NPD

Because the H_2 plasma showed better DREs for decontamination of DNT, we tested it first for decontamination of TNT. As shown in Table 13, a CW, pulsed, and a CW/pulsed combination of H_2 plasmas show DREs ranging from 95.01% to 99.3% with a TNT loading of ~20 mg. The analyses were carried out using a gas chromatograph with an NPD. Runs 1 through 4 in Table 13 show the results of tests run with power wattage increasing from 100 to 500 W, continuous wave, and time decreasing from 45 min (100 W) to 8 min (500 W). The DREs are 99.08%, 97.51%, 97.02%, and 99.50% for Runs 1 through 4. Runs 5 through 11, with pulsed plasmas only or combinations of CW and pulsed plasmas, did not improve DRE greatly. For example, using CW for 10 min followed by an on/off duty cycle of 3 ms/6 ms for 13 min (Run 7) resulted in a DRE of 99.02%. The results suggest that parameters optimized for DNT are not the most adequate parameters for TNT decontamination. Therefore, four different gas plasmas—H_2O, H_2, O_2, and Ar—were tested for TNT decontamination under similar conditions, i.e., 200 W, CW, and 23 to 25 min of treatment time.

Table 13. Decontamination of TNT with H_2 Plasma

Run #	Wattage	Plasma Mode	Time (min)	DRE (%)
1	100	CW	45	99.08
2	200	CW	23	97.51
3	300	CW	14	97.02
4	500	CW	8	99.50
5	300	3 ms/6 ms	45	98.78
6	500	3 ms/6 ms	40	98.68
7	500	CW/3 ms/6 ms	10/13	99.02
8	500	CW/20 ms/65 ms	5/18	95.77
9	500	CW/10 ms/75 ms	10/110	95.01
10	500	CW/5 ms/80 ms	12/318	94.50
11	300	3 ms/6 ms	120	99.27

The results using the four plasmas are summarized in Table 14. As shown in the table, O_2 plasma resulted in the highest DRE followed by H_2O and H_2 plasmas. The least effective gas is argon. But the DREs are relatively similar, ranging from 96.37% to 98.34%. O_2 plasma, with the highest DRE, was then tested with different parameters, including power wattage, time, and pulse frequency, to optimize the condition.

Table 14. Comparison of H_2, O_2, Argon, and H_2O Plasmas for Decontamination of TNT

Gases	Wattage	Time	DRE (%)
H_2	200	23	97.31
O_2	200	25	98.34
Ar	200	23	96.37
H_2O	200	23	97.47

Table 15 summarizes results, showing DREs ranging from 95.80% to 99.47% for O_2 plasma treatment. Run 4, with 500 W and CW for 8 min, is the most effective, with 99.47% DRE. Run 3, with 300 W and CW for 10 min, is the least effective, with 95.80% DRE. Until now, the DREs for TNT have been limited to less than 99.9% with various plasma gases and pulsed/CW combination. It is suspected that, once the polymerization of TNT fragment initiates, a minute amount of the trapped and unreacted TNT will be difficult for plasma to reach. As described previously in this report, using milder conditions with longer treatment time can improve the DRE further. The TNT is more prone to trapping the unreacted material than the DNT, probably because more heat is generated from the reaction between plasma and TNT than between plasma and DNT.

Table 15. Effects of Wattage, Plasma Mode, and Treatment Time on DRE for O_2 Plasma Decontamination of TNT

Run #	Wattage	Plasma Mode	Time (min)	DRE (%)
1	100	CW	45	97.53
2	200	CW	25	98.34
3	300	CW	10	95.80
4	500	CW	8	99.47
5	500	CW/10 ms/70 ms	10/110	99.11

Extremely high DREs (99.81% to 99.997%) are obtained using long treatment time with mild plasma conditions as shown in Table 16. All three types of plasma gases (H_2, O_2, and H_2O) are used. Two tests with O_2 plasma (Runs 3 and 5) are the first tests with DRE exceeding 99.99% for decontamination of TNT. Two tests of H_2O plasma (Runs 2 and 4) show DREs of 99.97% and 99.9% for duty cycles of 3 ms/12 ms over 4 h and 5 ms/12 ms over 3 h, respectively. H_2 plasma, on the other hand, shows relatively lower DRE, even with longer treatment time compared with O_2 plasma. The results suggest O_2 plasma with milder treatment conditions, lower duty cycle, and longer treatment times is more effective in decontaminating TNT. As shown in Runs 3 and 5, 300 W and on/off duty cycles of 2 ms/14 ms for 3 h and 3 ms/12 ms for 5 h both obtain DREs exceeding 99.99%.

Table 16. Extremely High DREs Are Achieved with Long Treatment Time and Mild Plasma Conditions

Run #	Gases	Wattage	Duty Cycle	Time (h)	DRE (%)
1	H_2	300	3 ms/12 ms	4	99.81
2	H_2O	300	3 ms/12 ms	4	99.97
3	O_2	300	3 ms/12 ms	3	>99.99[a]
4	H_2O	300	5 ms/12 ms	3	99.90
5	O_2	300	2 ms/14 ms	5	99.997

[a]Exceeds detection limit.

2.2.2.2 Decontamination Product Analysis with On-line MS

The MS spectra of TNT decontamination are similar to DNT decontamination. The major products are N_2, CO_2, and H_2O for O_2 and H_2 plasma decontamination of TNT as shown in Figures 22 and 23. The minor products are NO_x, mainly NO (Figures 24 and 25). No unreacted TNT is detected. The major difference between spectra of TNT and DNT is the mass #18 peak (H_2O). During DNT decontamination, no matter what gases were used, the #18 abundance always showed a maximum at the same time as other peaks' maxima (#28 and #44). For TNT decontamination, we observed a maximum when H_2 plasma was used, but a minimum when O_2 plasma was used. This suggests that oxygen radicals in the plasma are more selective toward carbon or nitrogen oxidation than toward hydrogen oxidation. We do not understand the exact mechanism for the sudden change of oxidation selectivity. The minimum position coincides with

other maximum peaks, which indicates that the heat generated by the fast reaction during the peak period may be the cause.

Another difference between spectra of TNT and DNT is the relatively lower portion of NO_2 in NO_x (Figures 24 and 25). As reported in the previous section, the ratio of NO to NO_2 peak area is about 10:1 to 15:1 for DNT. In the case of TNT, the NO to NO_2 ratio is similar to that of DNT with H_2 plasma, but the ratio increases dramatically when O_2 plasma is used. It is expected that the NO to NO_2 ratio should increase under reductive atmosphere (e.g., in H_2) and decrease under oxidative atmosphere (e.g., in O_2). The trend is somewhat reversed when the plasma system is applied as shown in Figures 24 and 25; however, the total NO_x abundance is reduced when H_2 plasma is used for TNT decontamination.

2.2.2.3 Light Emission Monitoring with UV Spectrometer

The emission spectra of TNT reacting with H_2O, H_2, and O_2 plasmas, as shown in Figures 26, 27, and 28, are similar to the emission spectra of DNT reacting with the same plasmas (Figures 18, 19, and 20). Three major peaks are again 482.4 nm, 517.5 nm, and 559.6 nm. And their intensities increase with time to a maximum, then decrease to a level close to the initial intensities. The peaks that changed most dramatically during the decontamination process are the same for DNT and TNT. They are 336.5 nm, 355.9 nm, and 606.8 nm for H_2 plasma (Figures 18 and 26) and O_2 plasma (Figures 20 and 28). But the signature peak at 387.5 nm, shown in Figure 19 for DNT reaction with H_2 plasma, did not decrease to the original intensity when TNT was used. The spectra are shown in Figure 27. In fact, it is hard to differentiate the three plasma treatments with TNT based on the emission spectra. The only exception is the peak at 387.5 nm for the H_2 plasma, which does not decrease as fast as in other reactions between TNT and plasmas. But the UV emission spectrometer is still an effective tool to monitor the decontamination process using the selected peaks. As shown in Figure 27, the peak at 387 nm is the most prominent peak to monitor the process because its intensity changed more than an order of magnitude while other peaks had relatively smaller changes.

2.2.3 Tests of DNT and TNT Loaded on Full-size Shell Surfaces

Both DNT and TNT were tested on all surfaces of an 81-mm shell surface. The explosives were loaded onto the shell casing surface by heating the shell to ~90 °C. Weighed samples were then placed on top of the shell surface, which melts the explosives because its temperature exceeds the melting temperature of explosives. We then mechanically rotated the shell. The explosives flow on the surfaces and solidify when the shell surface cools below the melting point of DNT or TNT. Only O_2 plasma was tested to decontaminate the explosives. After the plasma treatment, the shell was put in a container with 1.2 L of acetonitrile overnight. The resulting solution was then injected into the GC/NPD to measure the concentration of solution. Because of the large solvent volume and the small amount of DNT or TNT residue, the explosive residue concentration was below the detection limit of NPD, 0.2 µg/mL. The solutions were then concentrated by a rotating evaporator from 1.2 L to ~50 mL. Table 17 summarizes the results of five tests. The concentration of the concentrated solution was analyzed again by GC/NPD. The residue amount was determined and DRE was calculated. As shown in Table 17, Run 1, with

0.44 g of DNT loaded on the outside surface of the shell, achieved 99.99% DRE with 3-h treatments of O_2 plasma at 300 W and a duty cycle of 5 ms/12ms.

Table 17. Tests of O_2 Plasma for Decontamination of DNT and TNT Loaded on a Full-Size 81-mm Shell

Run #	Wattage	Plasma Mode	Time (h)	Explosive	Surface Loading (mg)	DRE (%)
1	300	5 ms/12 ms	3	DNT/outside	440	99.99
2	300	5 ms/12 ms	3	TNT/outside	500	99.97
3	300	5 ms/12 ms	3	TNT/inside	500	99.98
4	300	3.3 ms/14 ms	4	TNT/both	1,000	99.95
5	300	2 ms/15 ms	5	TNT/both	1,000	99.94

Run 2, replacing DNT with TNT on the outside surface of the shell, achieved slightly lower DRE, 99.97%, using the same parameters as were used in Run 1. This suggests that it is relatively more difficult to decontaminate TNT than DNT and achieve extremely high DREs. A DRE of 99.98% was achieved when 0.5 g of TNT was loaded on the inside surface of the shell in Run 3, suggesting that the inside surface of a full-size shell is relatively easier to decontaminate. This result is beneficial because most TNT residue will be on the inside surface after the steam-melting step is done to recover the explosives. TNT loaded on both the inside and outside surfaces of shells was tested in Runs 4 and 5. Duty cycles were reduced to 3.3 ms/14 ms and 2 ms/15 ms for Runs 4 and 5, respectively, but the treatment times were increased to 4 hours for Run 4 and 5 hours for Run 5. The DREs obtained were 99.95% and 99.94%. This is the first successful demonstration of TNT decontamination on an 81-mm shell with the nonthermal plasma process. Although the highest DRE for TNT on the full-size shell was 99.95% (Run 4), it is a one-step clean decontamination using only electricity and generating a negligible amount of exhaust gases.

2.2.4 Decontamination of RDX and Comp B

2.2.4.1 Direct Decontamination Analysis with HPLC/UV

Due to the decomposition of RDX at the injector port of GC, the analysis of RDX and Comp B was carried out using a high-pressure liquid chromatograph (HPLC) with the UV detector. According to previous results that H_2 plasma showed better DREs for decontamination of DNT and O_2 plasma was more effective for TNT decontamination, the decontamination of RDX and Comp B was tested with three plasmas, O_2, H_2O, and H_2. The results are summarized in Tables 18 and 19 for RDX and Comp B, respectively.

As shown in Table 18, all three plasmas can effectively decontaminate RDX to above 99.999% DRE with about 20 mg of samples. Continuous wave or pulsed modes are both efficient, but more time was required for the pulsed mode.

Table 19 shows the results of Comp B decontamination with three plasmas. Since Comp B contains 60% TNT and 40% RDX, both residues of RDX and TNT after plasma decontamination were analyzed. The calculation of DREs for RDX and TNT were based on the weights in the samples (~20 mg). Although all three plasmas were effective for RDX decontamination with pure RDX samples, the decontamination efficiencies of RDX in Comp B with three plasmas were somehow different. When 200 W power was used, the order of DRE for RDX in Comp B was $O_2 > H_2O > H_2$. However, the order was $H_2O > H_2 > O_2$ when 300 W power was used. For TNT destruction in Comp B samples, all three plasmas achieved highest destruction efficiency (>99.9997%), based on the detection limit, when 200 W power was used. But when 300 W power was used, H_2 plasma showed somewhat lower efficiency (99.975%) for TNT removal in Comp B samples.

Table 18. Decontamination of RDX with O_2, H_2O, and H_2 Plasmas

Run #	Plasma	Wattage	Plasma Mode, Time (min.)	Residue	DRE (%)
1	O_2	200	CW, 120	ND	>99.999
2	O_2	300	CW, 30	ND	>99.999
3	O_2	300	3 ms/6 ms, 420	ND	>99.999
4	H_2O	200	CW, 60	ND	>99.999
5	H_2O	300	CW, 30	ND	>99.999
6	H_2	200	CW, 90	ND	>99.999
7	H_2	300	CW, 30	ND	>99.999

Detection limit = 0.1 µg/mL.

ND = Not detectable.

Table 19. Decontamination of Comp B with O_2, H_2O, and H_2 Plasmas

Run #	Plasma	Wattage	Plasma Mode, Time (min)	Residue		DRE (%)	
				RDX	TNT	RDX	TNT
1	O_2	200	CW, 60	ND	ND	>99.995	>99.997
2	O_2	300	CW, 30	5.96 µg	ND	99.929	>99.997
3	H_2O	200	CW, 60	1.632 µg	ND	99.979	>99.997
4	H_2O	300	CW, 30	ND	ND	>99.995	>99.997
5	H_2	200	CW, 70	5.60 µg	ND	99.934	>99.997
6	H_2	300	CW, 35	1.024 µg	2.988 µg	99.987	99.975

Detection limit = 0.1 µg/mL.

ND = Not detectable.

A comparison of Tables 19 and 18 indicates that RDX decontamination is relatively more difficult to achieve in Comp B samples than in pure RDX samples. It is expected that TNT will react with plasma faster than RDX because of its lower boiling point. It is our speculation that the heat released from the TNT decontamination causes curing of RDX, which makes it more difficult to remove.

To compare the decontamination of TNT with RDX and Comp B directly, additional experiments of TNT with O_2 plasma were carried out under similar conditions, continuous wave 200 W for 60 min and 300 W for 30 min. The results are summarized in Table 20. The DREs for TNT are lower than the DREs of TNT in Comp B samples, which is opposite the phenomenon of RDX in Comp B samples. Because the TNT in Comp B is more dispersed because of the additional RDX compound in the mixture sample, it is speculated that the heat effect is minimized, thus achieving higher destruction efficiencies.

Table 20. Decontamination of TNT with O_2 Plasma

Run #	Plasma	Wattage	Plasma Mode, Time (min)	Residue	DRE (%)
1	O_2	200	CW, 60	2.64 µg	99.987
2	O_2	300	CW, 30	8.86 µg	99.958

Detection limit = 0.1 µg/mL.

ND = Not detectable.

2.2.4.2 Decontamination Product Analysis with On-Line MS

The MS spectra of RDX decontamination are quite different from the spectra of TNT decontamination. Figures 29 and 30 show the abundance of Mass #18, 28, and 44 over time for the decontamination of RDX with O_2 and H_2 plasmas, respectively. The major products are N_2, CO_2, and H_2O, but the peaks are much lower and broader than the peaks shown in Figure 31. The highest peak for RDX decontamination is mass #18 (H_2O) as opposed to mass #28 (N_2) in the case of TNT. This result suggests that RDX reaction with plasma is much slower than the reaction between TNT and plasma, although the major products are the same, N_2, CO_2, and H_2O.

The MS spectra of Comp B can be expected to be the mix of TNT and RDX. As shown in Figure 32, MS spectra of O_2 plasma with Comp B shows two peaks. The earlier one indicates the reaction of TNT with plasma and the second one of RDX with plasma. Similar spectra were obtained with H_2 and H_2O plasmas. In fact, the two peaks indicating the mixture of TNT and RDX are much clearer in the RDX spectra. Figures 33 through 35 show NO_x abundance versus time for O_2, H_2O, and H_2 plasmas for Comp B decontamination, respectively.

As shown in Figures 33, 34, and 35, all three tests showed negligible NO_x formation and two distinct peaks. It is interesting that none of the second peaks is larger than the first peaks in all of these tests. RD_X contains six nitrogen atoms in the molecule compared to only three in the

TNT molecule. It is expected that RDX would generate more NO_x than TNT in Comp B samples.

2.2.5 *Economic Analysis*

Because plasma technology is effective at decontaminating both TNT and Comp B explosives, the economic analysis focused on the cleaning of shell casings containing these two explosives. According to the economic evaluation conducted by TVA, material costs represent the major part of the operating cost, $60.87/metric ton, of the HGD process. Fuel oil is the dominant portion (91%) of these material costs and is not required by the nonthermal plasma process. The electricity required per week (40 h/wk) for the plasma process is estimated to be 96 kWh and, assuming the current system is being scaled up to treat 36 175-mm projectiles in a 1-h batch, 40 batches each week. The overall electricity required for the plasma process is less than 5% of the electricity needed for the HGD process to treat the same amount of projectiles. Assuming everything else is equal, including personnel cost, sampling cost, maintenance material, and miscellaneous supplies, our estimate of the operating costs of the plasma process is $29.67/metric ton (48.7% of the HGD process). The operating costs for the HGD and the nonthermal plasma processes are compared in Table 21. Although the electricity projection is based on one shell system, we believe that scaling up to treat 36 projectiles in one batch will not require 36 times the power of a one-shell system. (The energy efficiency of the plasma system to treat multiple objects is expected to be higher than the energy efficiency to treat a single object, based on our experience.) It is estimated that the current plasma process, after being scaled up, can save at least 50% of the operating cost as compared to the HGD process.

Table 21. Comparison of Operating Costs for HGD and Nonthermal Plasma Processes

Operating Cost	Nonthermal Plasma	HGD
Fuel	None	$29.59/metric ton
Electricity	$0.07/metric ton	$1.67/metric ton
Others (personnel, sampling, maintenance, material and supplies)	$29.61/metric ton	$29.61/metric ton ($25.21+$3.19+$1.20)
Total	$29.67/metric ton	$60.87/metric ton

3.0 SUMMARY

3.1 HYDROTREATMENT OF CHEMICAL WASTES

Three percent $Pt/\eta\text{-}Al_2O_3$ is active and relatively stable for hydrogenation of CEES. At 250 °C, HDS and HDC of CEES is stable for 20 h with 25:1 H_2 to CEES ratio and 24,000 $cm^3/h/g$ space velocity. More stable and active HDS and HDC of CEES are achieved over the $Ni\text{-}Mo/\gamma\text{-}Al_2O_3$ catalyst. At 300 °C, complete conversion of CEES is maintained for 100 h with gas composition of H_2:CEES: He=10:0.33:89.7 and 24,000 $cm^3/h/g$ cat space velocity. The reaction is 98% selective to pure hydrocarbon products (ethylene and ethane) and 2% to ethyl mercaptan. Much

less concentration of chlorinated hydrocarbon (chloroethane) than the concentration of sulfur-containing compounds (diethyl sulfide and ethyl mercaptan) in the product stream suggests that HDC is faster than HDS of CEES over Ni-Mo/γ-Al_2O_3. Two di-sulfur-containing compounds—1,2-bis (ethylthio) ethane and 1,4-dithiane—were detected during the reactions with short residence times. This indicates the reaction pathway of hydrotreatment of CEES is much more complicated than simple HDS and/or HDC reactions.

AC-supported catalysts are active and selective for hydrotreating CEES. Above 99.5% selectivity to hydrocarbons was achieved over Ni-Mo/AC at 300 °C. Major HC products are ethylene and ethane. The activity order of various catalysts is Ni-Mo/AC>Ni-Mo/Al_2O_3>3% Pt/η-Al_2O_3 for stable hydrotreatment of CEES. A much higher H_2:CEES ratio above the stoichiometric requirement is needed to maintain a high and stable selectivity to hydrocarbons.

The longevity of the catalytic hydrotreatment of CEES has been demonstrated over Ni-Mo/AC and Pt/MZ391 catalysts. From 99.996% to 99.998% destruction efficiency is achieved. These results suggest that hydrotreatment is promising for the detoxification of mustard gas. The investigation of reaction pathways indicates that the hydrotreatment of CEES is complex. More research is needed to understand this reaction mechanism, which is important to further improve the destruction efficiency of the process and the stability and activity of the catalysts.

3.2 Plasma Technology for Surface Cleaning

We have successfully demonstrated that the RF plasma technology is very effective for the removal and destruction of DNT, TNT, RDX, and Comp B on shell surfaces. DREs of DNT measured directly by NPD are mostly above 99%. The results suggest that mild plasma conditions favor higher DREs. Under the same decontamination conditions, H_2 plasma is more efficient than O_2 plasma. The best three decontamination conditions are 100 W with 6 ms/3 ms cycle, 75 W with continuous wave, and 200 W with 3 ms/6 ms cycle of H2 plasma. The best destruction efficiency reported is 99.86% for DNT decontamination.

O_2 plasma, on the other hand, shows better DREs for the decontamination of TNT. Product analysis with an on-line mass spectrometer indicates that the plasma process is environmentally benign for decontamination of DNT and TNT explosives. The major decontamination products are N_2, CO_2, and H_2O with a small amount of NO_x, mainly NO. No unreacted explosives were detected by MS, suggesting that the plasma process is effective not only for explosives removal but also for the destruction of explosives in one step.

Detection of light emission with a UV spectrometer for monitoring the decontamination of both DNT and TNT was demonstrated. The results suggest that the UV spectrometer is an excellent and economical tool to monitor the progress of the plasma process and to determine the decontamination endpoint. Although emission spectra are similar for various plasmas, peaks that change most dramatically during the process can be used most effectively to monitor the decontamination progresses. Special peaks for monitoring purposes are 387.5 nm and 656.7 nm for H_2 plasma; 336.5 nm, 355.9 nm, and 606.8 nm for H_2O plasma; and 336.5 nm and 355.9 nm for O_2 plasma with our system.

Explosives, DNT, and TNT loaded on a full-size shell were successfully decontaminated for the first time with the full-size shell plasma system. A DRE of 99.98% was achieved with O_2 plasma for 1.0 g of TNT loaded on both the inside and outside surfaces of an 81-mm shell casing. The decontamination of RDX and Comp B has also been demonstrated successfully with the cold plasma process. All tests with the pure RDX achieved >99.999% DREs. The DREs of RDX in Comp B were slightly lower. But two tests, O_2 plasma/200 W and H_2O plasma/300 W, achieved the maximum DRE of >99.995%. On the other hand, TNT in Comp B was more easily decontaminated than pure TNT samples. Five in six tests resulted in DREs >99.997%. It is estimated that the current nondestructive cleaning process can be scaled up to decontaminate the shell casings at an operating cost of less than $30/metric ton, approximately 50% of the cost for the HGD process reported earlier. These results suggest that the nonthermal plasma process is effective, efficient, and environmentally benign for decontamination of shell casings. Continuous investigation of scale-up for a multi-shell system is recommended.

4.0 RECOMMENDATIONS

Based on the successful test results of the single-shell plasma system, it is recommended that an automatic process be investigated to demonstrate the decontamination of tons of demiled shell casings. However, before scaling up the plasma decontamination process, additional investigations are needed to ensure that scale-up problems will be minimized.

The following tasks should be investigated:

1. Characterize the decontamination products and design/test a system with a larger plasma chamber to house multiple shell casings.

   Questions to be answered:

   - What is the material balance of the process? Possible products besides current non-quantified but detected major projects, N_2, CO_2, and H_2O include C1 to C7 hydrocarbons. Oxygenated hydrocarbons are also possible with O_2 plasma. Amines and ammonia could be formed during the decontamination of explosives with H_2 plasma. It is likely that no single analytical equipment could analyze all of the possible products.
   - What is the power efficiency of the multi-shell system? (Only one power source, matching network, and vacuum system are needed for this design. Energy coupling should increase the power efficiency per shell.)
   - Is the decontamination level similar for each shell?
   - If not, what are the times needed for each shell to be decontaminated?
   - Can the system decontaminate different sizes of shells and different explosives in one chamber?

2. Study the design and the hardware requirements for a multiple-chamber system.

   Questions to be answered:

- How can the number of power supplies, matching networks, and vacuum systems be minimized?
- Can solutions obtained to previous question be made to work with different chambers processing different shells?
- As the number of shells to be processed increases, how much effort and expense are required to process more chambers simultaneously with the minimum number of power supplies, matching networks, and vacuum systems?

3. Conduct a cost analysis of the automatic system using the information obtained in Tasks 1 and 2.

   Questions to be answered:

   - Can the scheduling and automation be both logistically and economically incorporated into the designs described?

4. Design a small-scale demonstration version to verify the accuracy of cost analysis.

   Questions to be answered:

   - Are design cost estimates correct?
   - Is automation possible?
   - Can cleaning and inspection be implemented?
   - Is there any safety and operating concerns?

REFERENCES

1. National Research Council, "Alternative Technologies for the Destruction of Chemical Agents and Munitions," 1992.

2. GAO, "Chemical Weapons Destruction. Issues Related to Environmental Permitting and Testing Experience," GAD/T-NSIAD-92-43, June 16, 1992.

3. Bonnet, M., P. Geneste, A. Guida, and D. Mamponya, J. Catal. 81, p. 79-84, 1983.

4. Zhou, X-L., Z.-J Sun, and J.M. White, J. Vac. Sci. Technol. A 11(4), p. 2110-2116, 1993.

5. Satterfield, C.N. "Heterogeneous Catalysis in Industrial Practice," p. 378, 1991.

6. Hagh, Bijan F., and David T. Allen, Innovative Hazardous Waste Treatment Technology Series. Vol. 2, Physical/Chemical Processes, Freeman, H.M., Ed., p. 45-53, 1990.

7. Kalnes, T.N., and R.B. James, Innovative Hazardous Waste Treatment Technology Series, Vol. 1, Thermal Processes, Freeman, H.M., Ed., p. 65-76, 1990.

8. Frankel, K.A., B.W.-L. Jang, G.W. Roberts, and J.J. Spivey, ISCD Proceedings, 1997.

9. Frankel, K.A., B.W.-L. Jang, G.W. Roberts, and J.J. Spivey, "Deactivation of Hydrodechlorination Catalysts: I-Experiments with 1,1,1-Trichloroethane," Appl. Catal., Vol. 205, 2001.

10. Ziolek, M., and P. Decyk. Studies in Surface Science and Catalysis 84, p. 1579-1586, 1994.

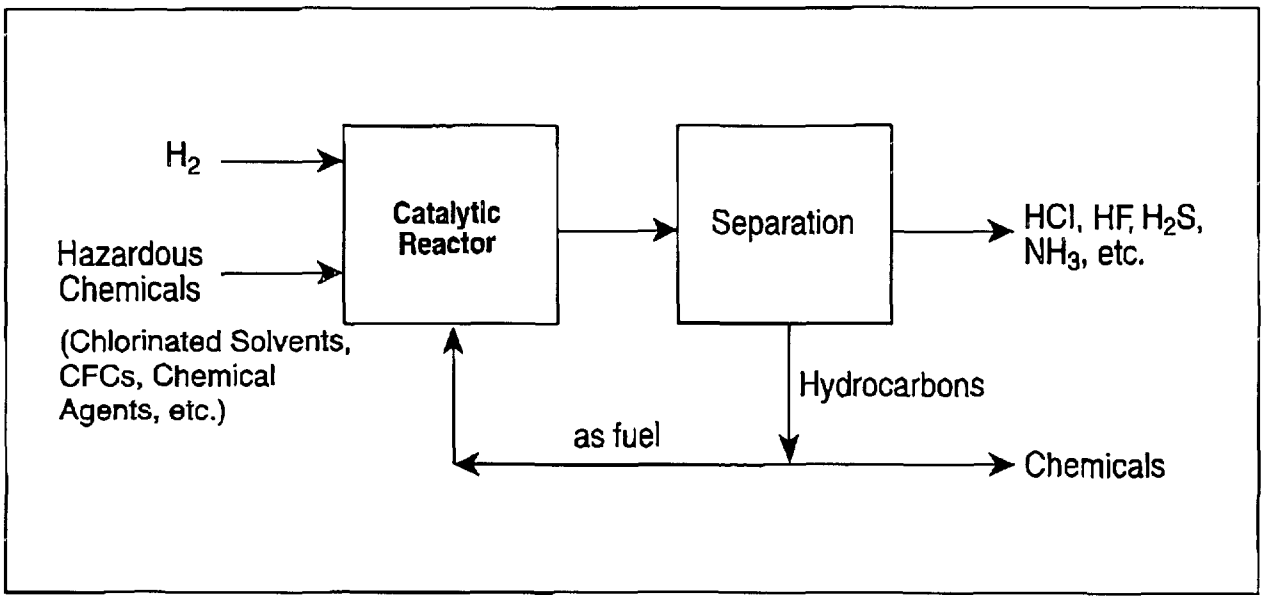

Figure 1. Process for removing heteroatoms from hazardous chemicals.

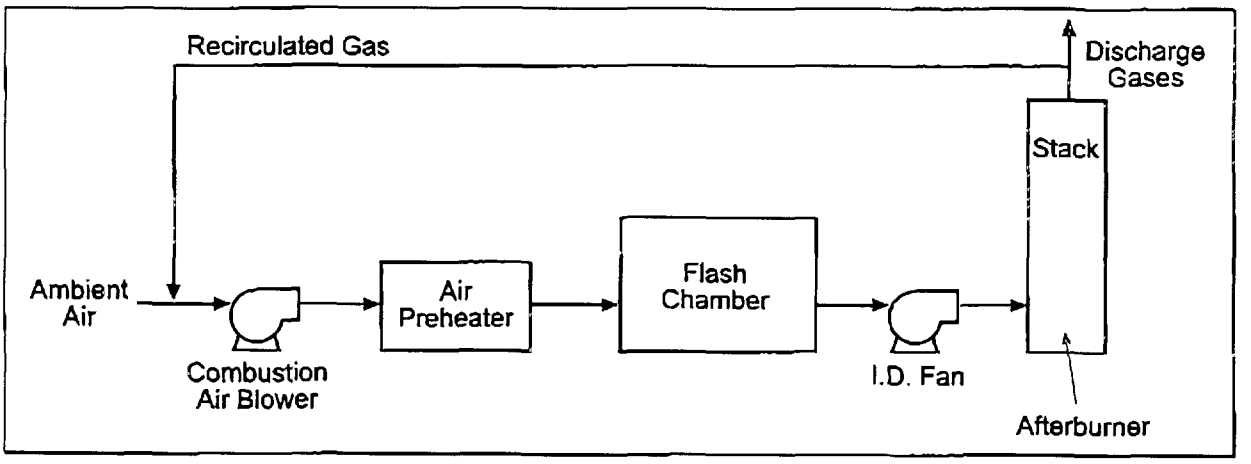

Figure 2. The HGD process.

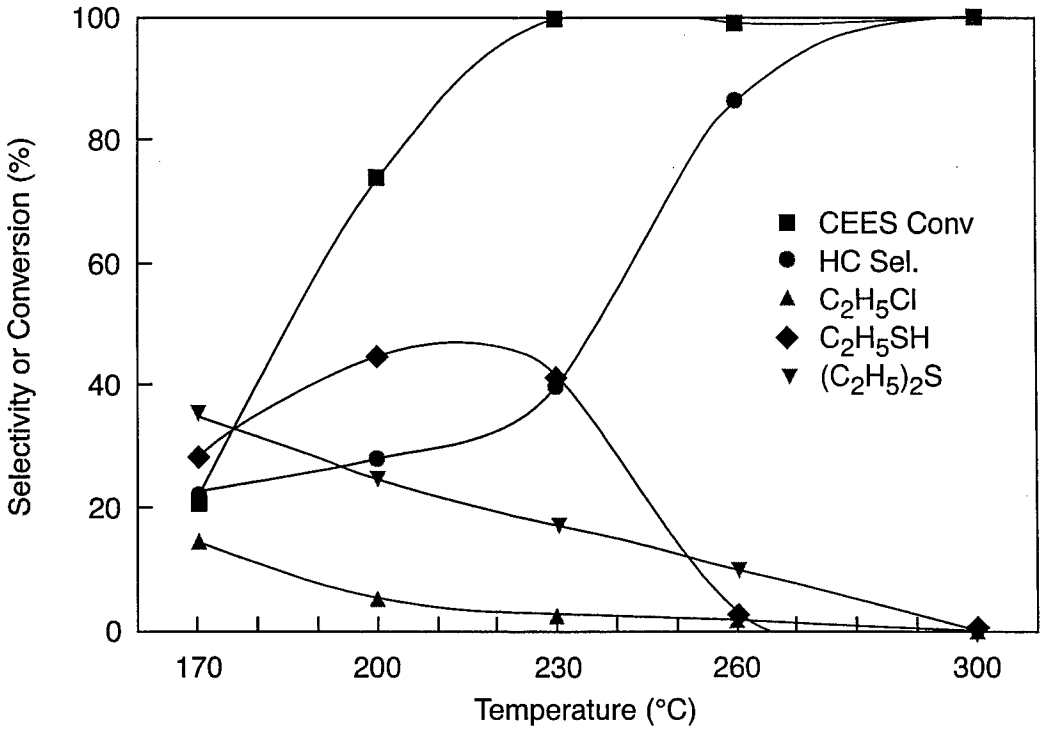

Figure 3. **CEES conversion and product distribution as a function of temperature over 3% Pt/η-Al_2O_3 catalyst at 200 cm^3/min, H_2/CEES/He=25/1/74, catalyst = 0.5 g.**

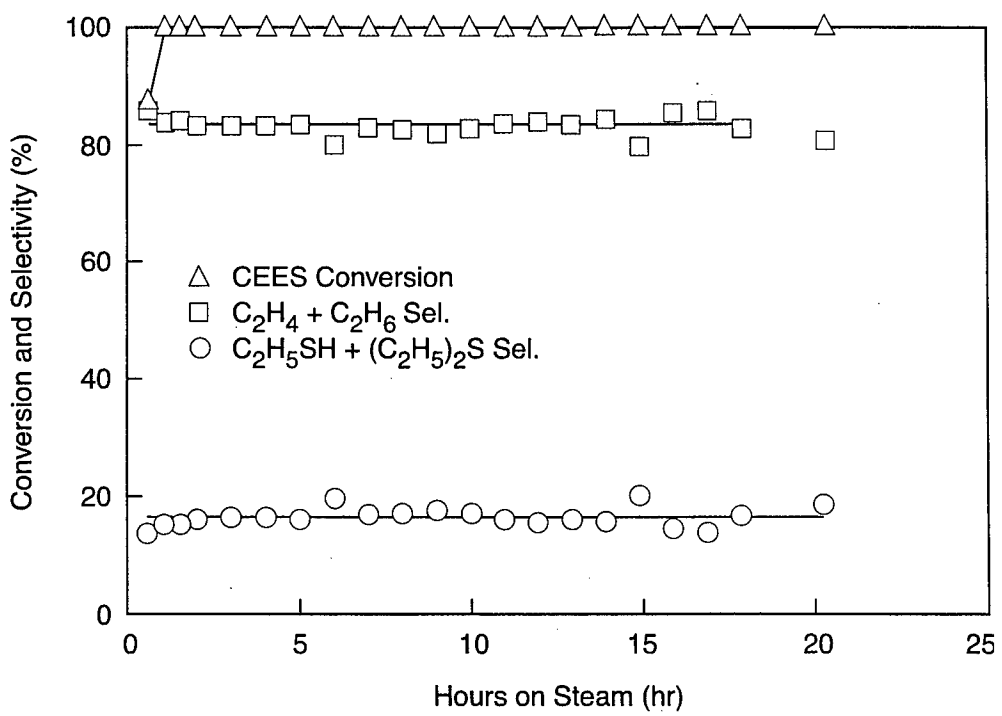

Figure 4. **Stability of 3% Pt/η-Al_2O_3 for hydrogenation of CEES at 250 °C, 200 cm^3/min, H_2/CEES/He=25/1/74, catalyst = 0.5 g.**

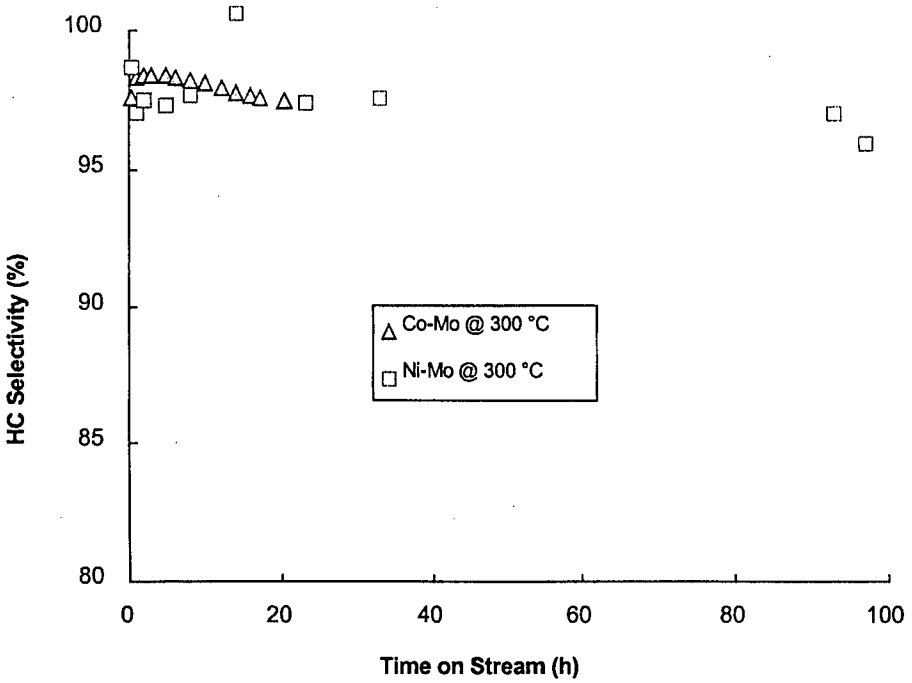

Figure 5. **Illustration of product selectivity to hydrocarbon formation during the first 20 h of CEES conversion over a Co-Mo catalyst and the first 100 h over a Ni-Mo catalyst at 300 °C, H_2/CEES/He=10:0.33:89.7; 24,000 cm^3/h.**

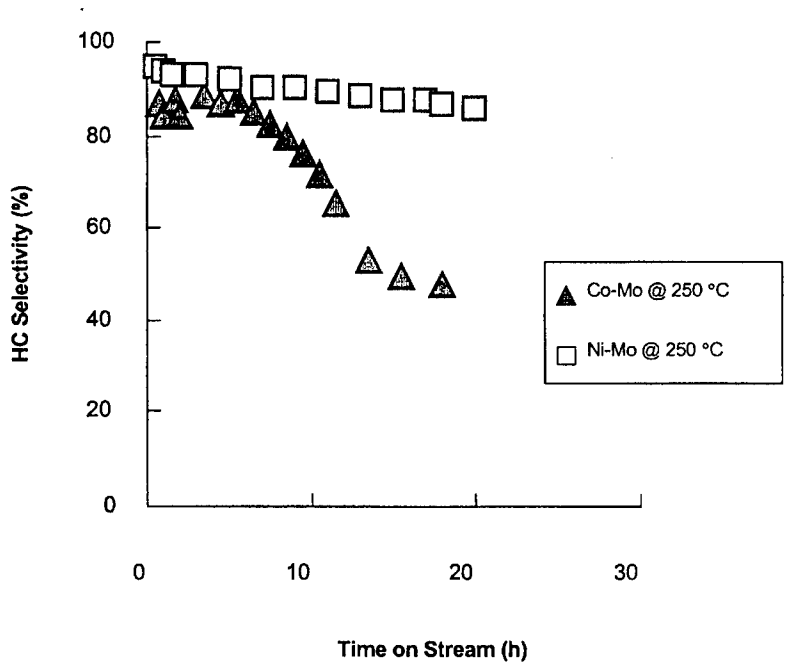

Figure 6. **Comparison of the activity of Co-Mo and Ni-Mo catalysts in the hydrotreatment of CEES at 250 °C expressed in terms of hydrocarbon product selectivity. H_2/CEES/He=10:0.33:89.7; 24,000 cm^3/h.**

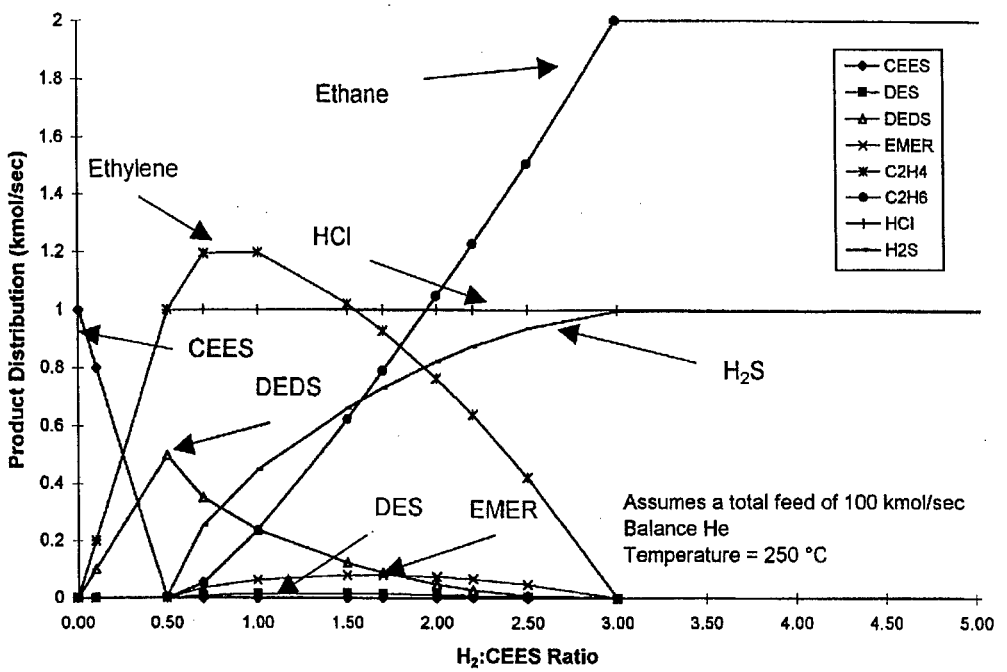

Figure 7. Products distribution of equilibrium of hydrotreatment of CEES at 250 °C.

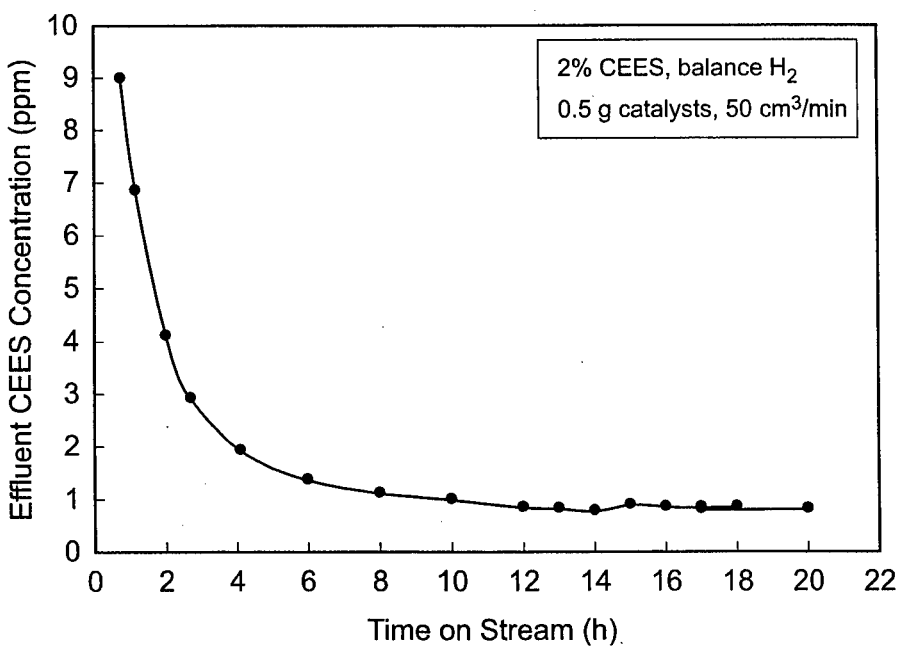

Figure 8. 99.996% destruction efficiency of CEES is achieved over Ni-MO-AC catalyst at 300 °C.

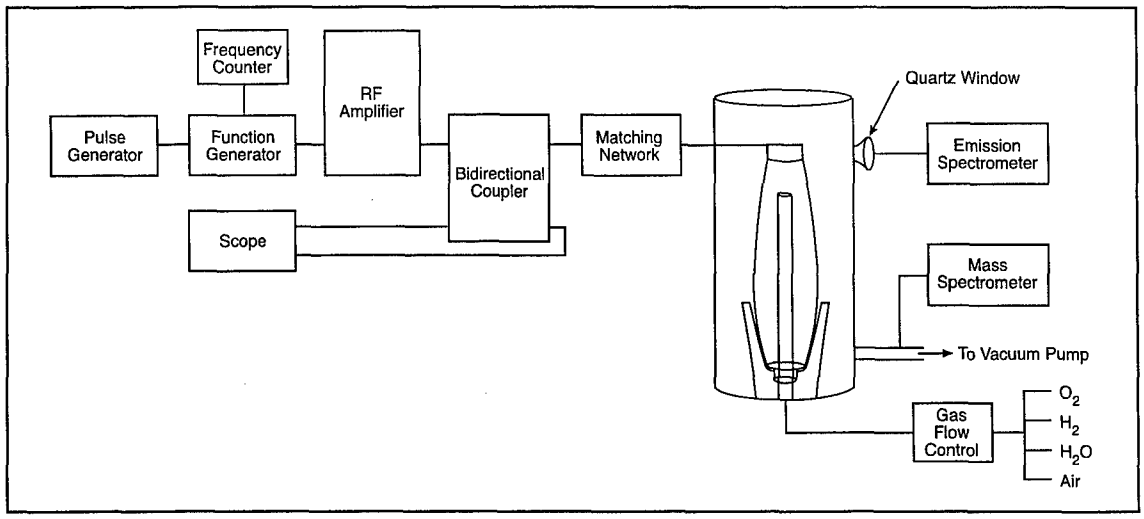

Figure 9. Schematic of RF plasma reactor system for full-size shells.

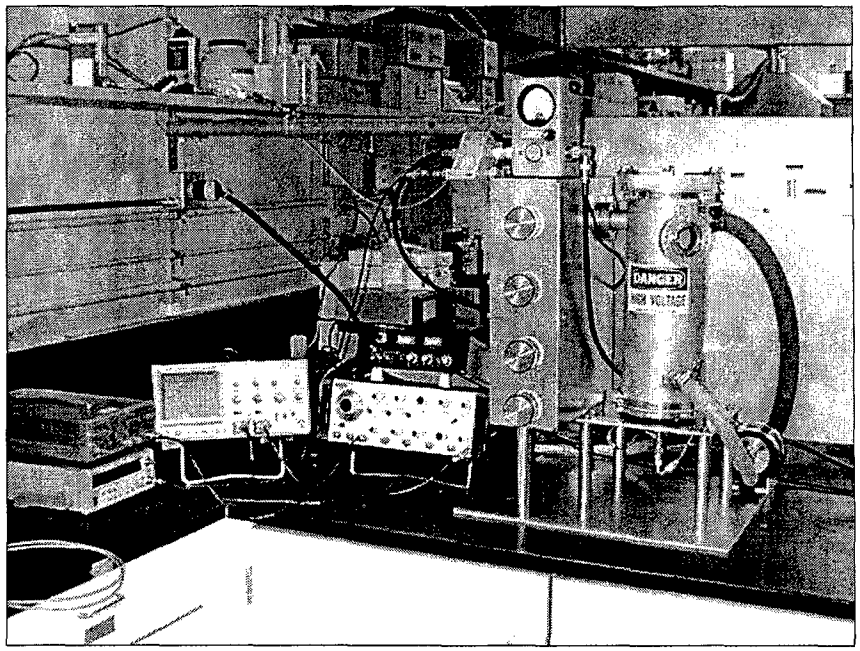

Figure 10. Plasma system for full-sized shell cleaning.

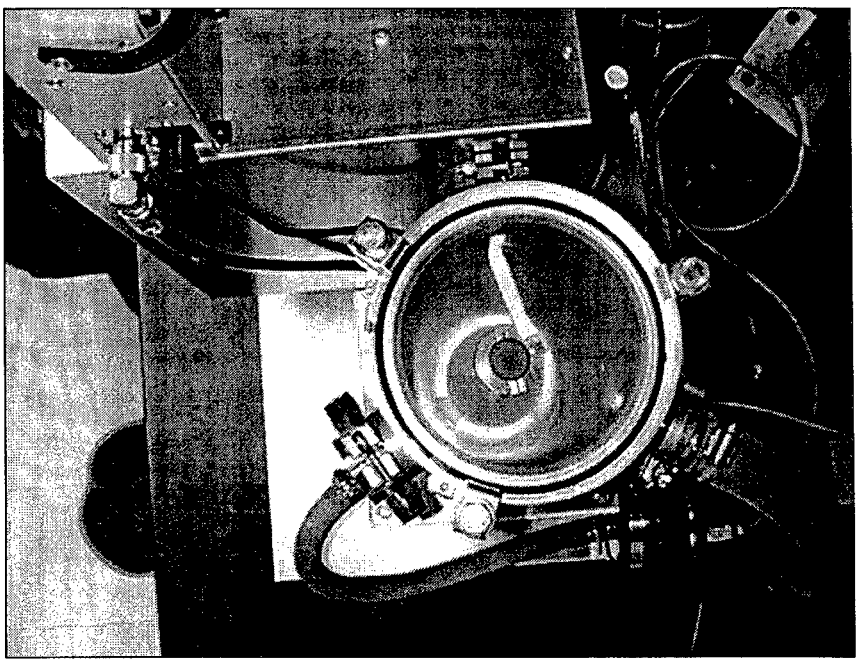

Figure 11. Top view of the plasma reactor during the continuous mode.

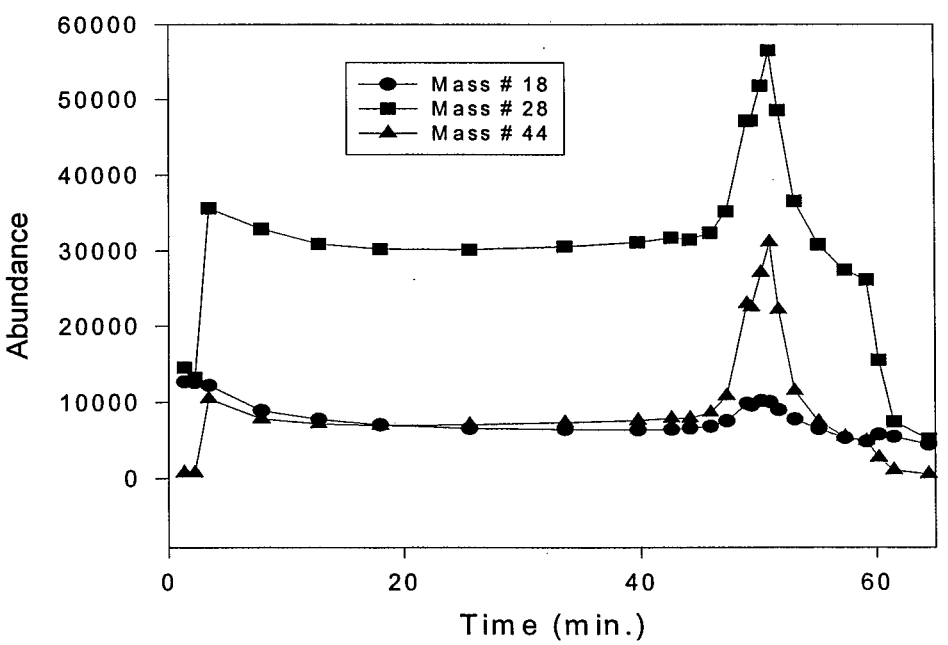

Figure 12. Abundance of mass numbers 18, 28, and 44 versus time during the H_2 plasma treatment of DNT. 200 W and 0.3 ms/0.6 ms on/off cycle.

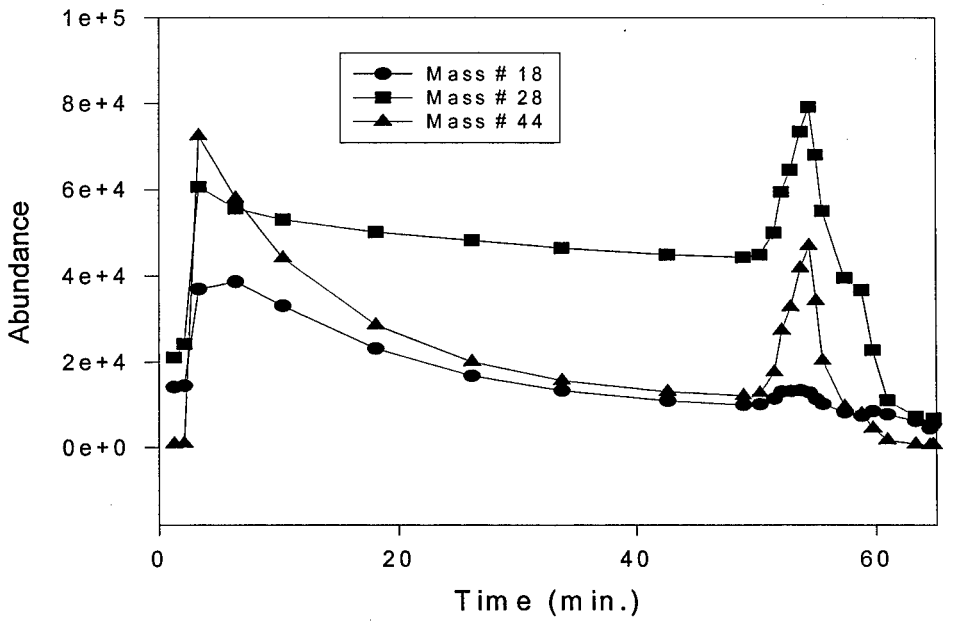

Figure 13. **Abundance of mass numbers 18, 28, and 44 versus time during the H_2 plasma treatment of DNT. 200 W and 3 ms/6 ms on/off cycle.**

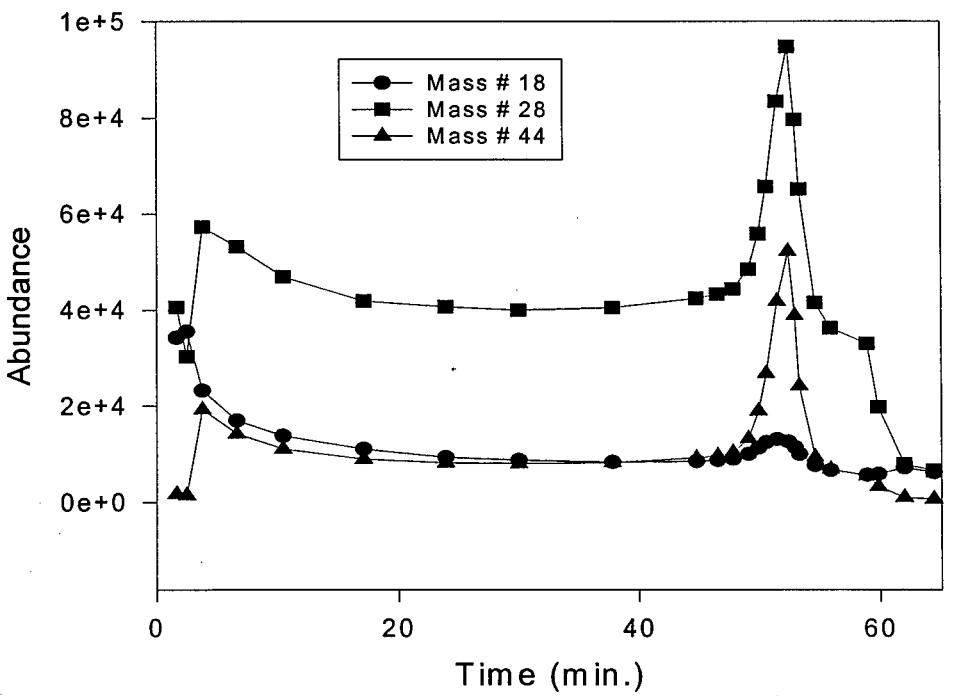

Figure 14. **Abundance of mass numbers 18, 28, and 44 versus time during the H_2 plasma treatment of DNT. 200 W and 30 ms/60 ms on/off cycle.**

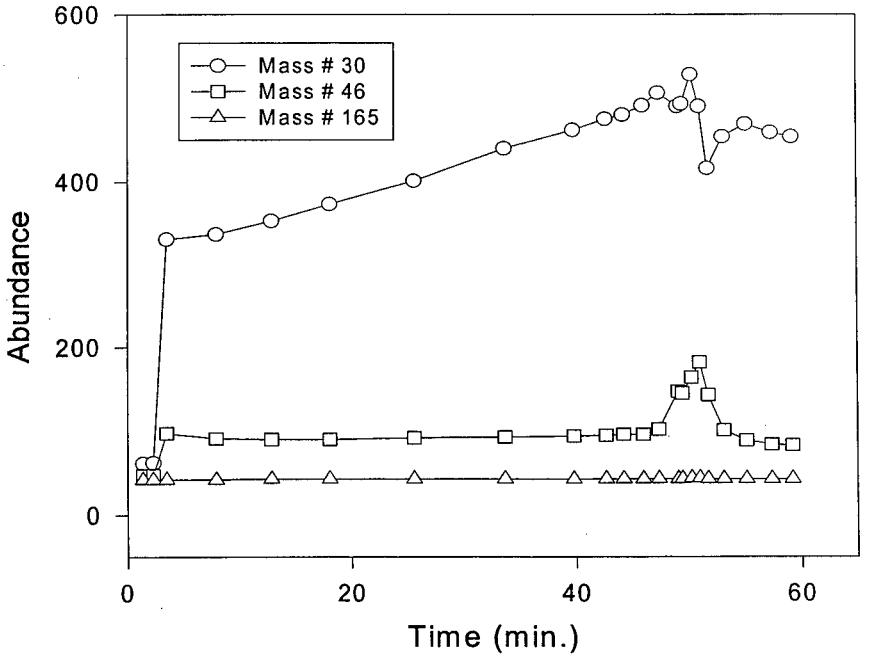

Figure 15. **Abundance of mass numbers 30, 46, and 165 versus time during the H_2 plasma treatment of DNT. 200 W and 0.3 ms/0.6 ms on/off cycle.**

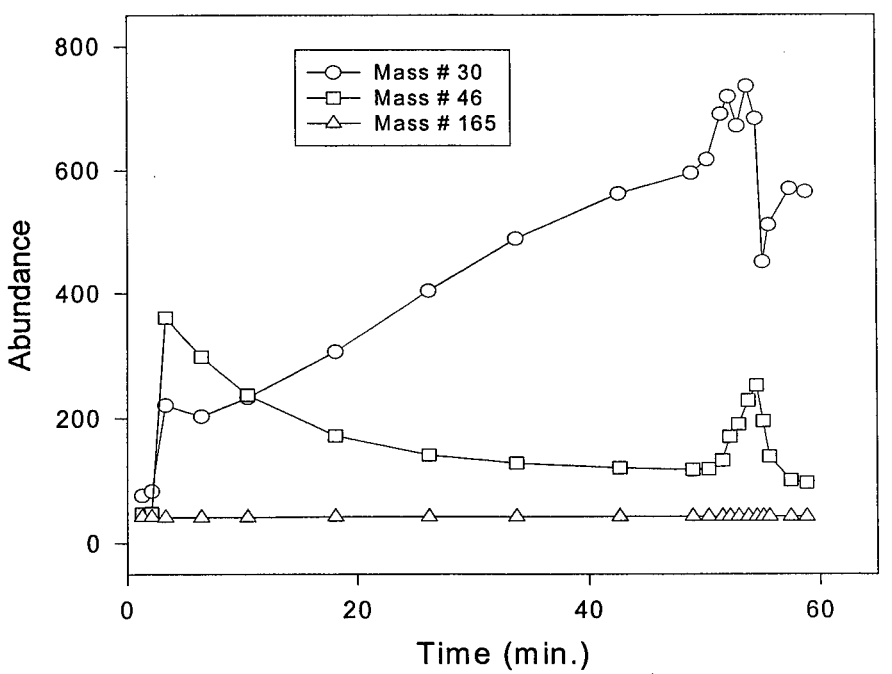

Figure 16. **Abundance of mass numbers 30, 46, and 165 versus time during the H_2 plasma treatment. 200 W and 3 ms/6 ms on/off cycle.**

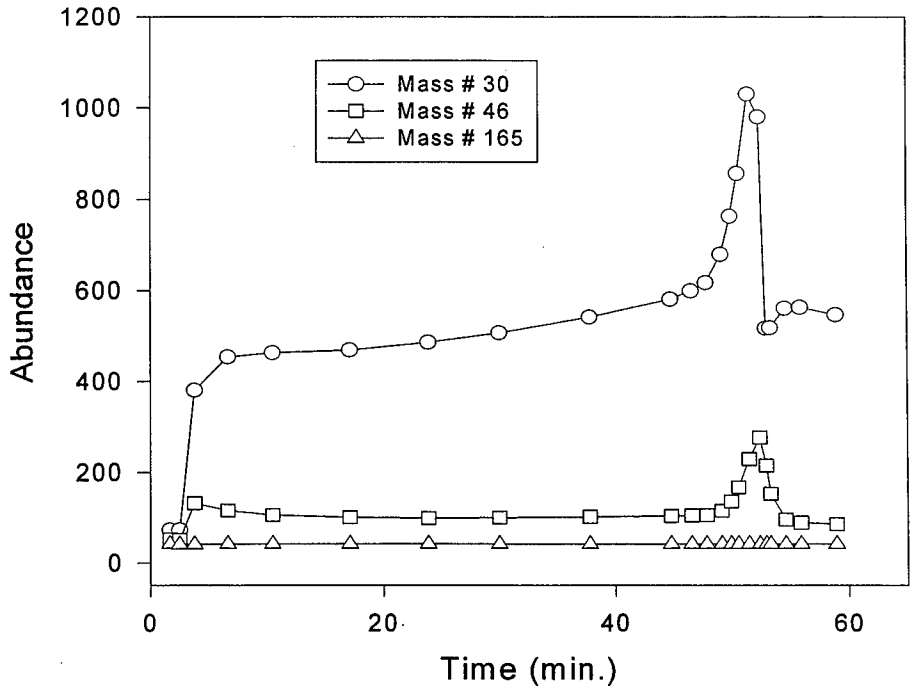

Figure 17. Abundance of mass numbers 30, 46, and 165 versus time during the H_2 plasma treatment. 200 W and 30 ms/60 ms on/off cycle.

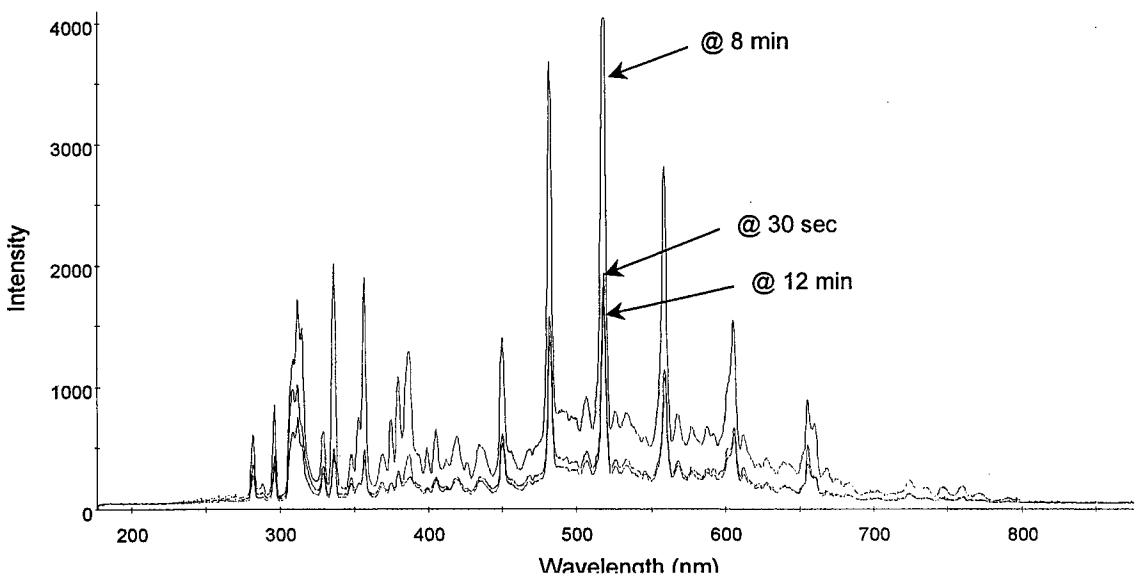

Figure 18. Emission spectra of H_2O plasma for decontamination of DNT, 200 W, 0.3 ms/0.6 ms.

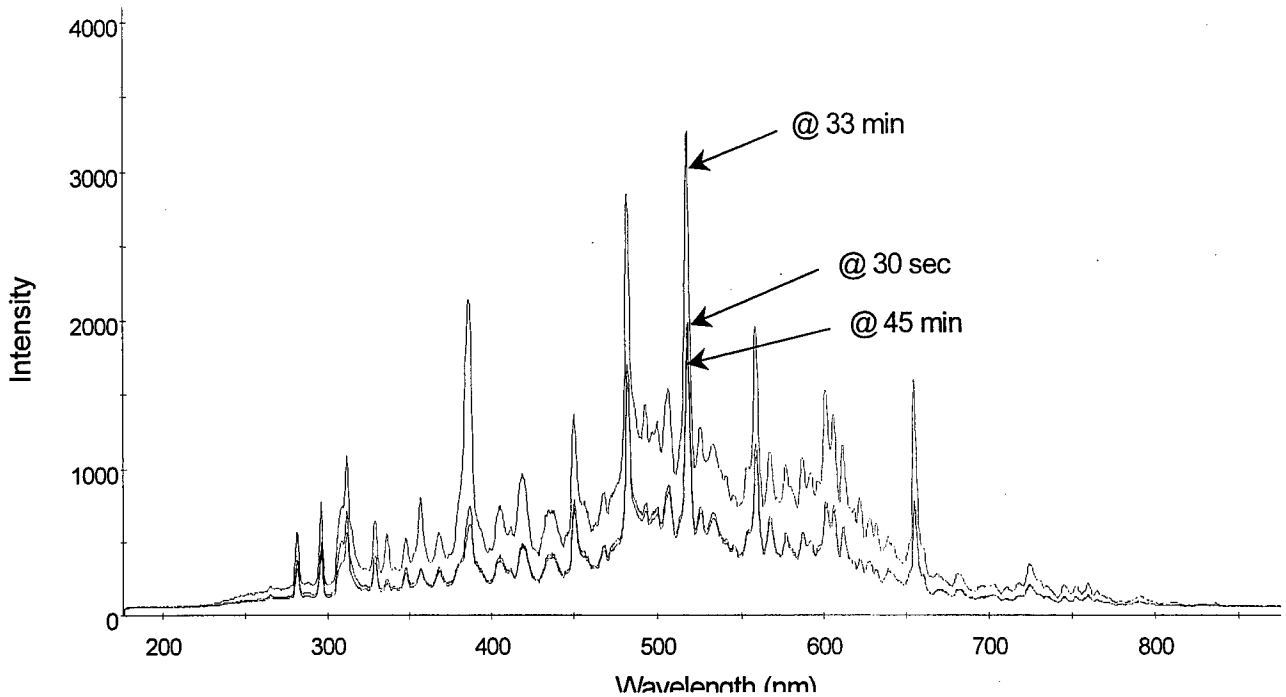

Figure 19. Emission spectra of H_2 plasma for decontamination of DNT, 100 W, CW

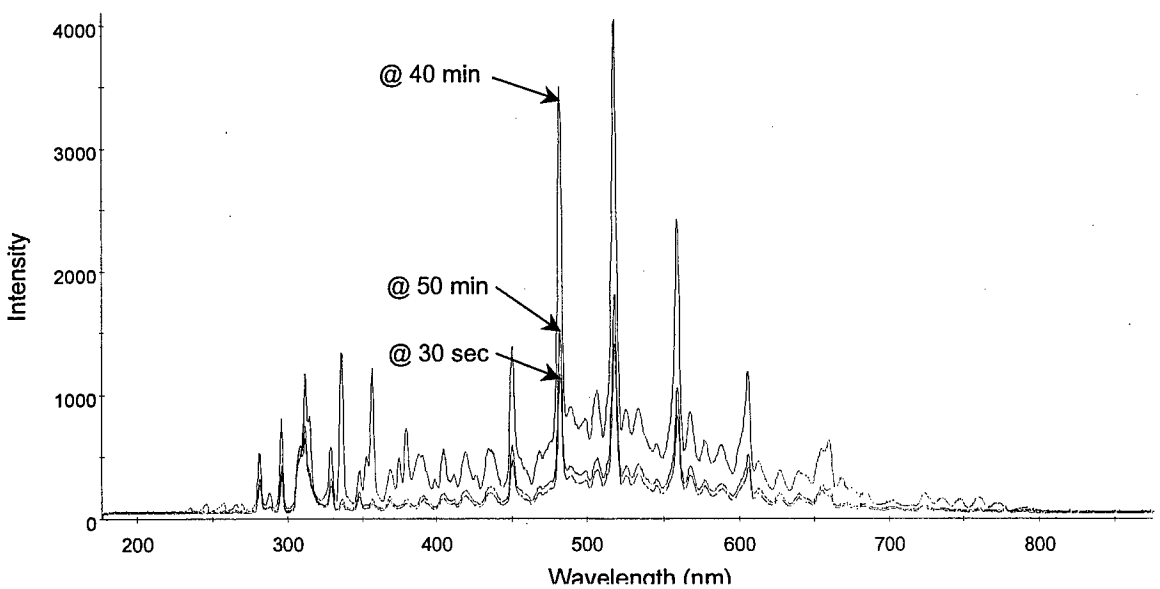

Figure 20. Emission spectra of O_2 plasma for decontamination of DNT, 200 W, 3 ms/6 ms.

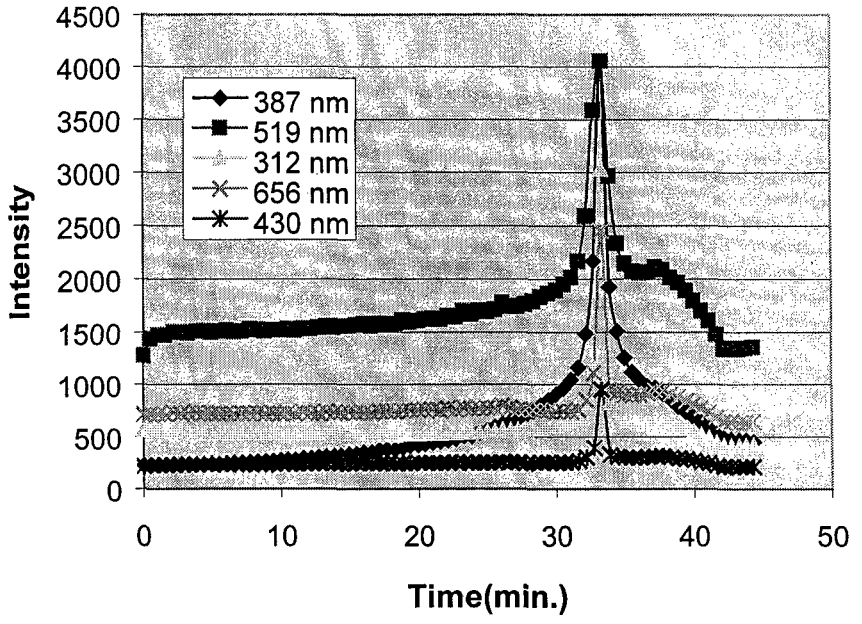

Figure 21. Emission spectra of selected peaks for H_2 plasma decontamination of DNT, 200 W, 0.3 ms/0.6 ms.

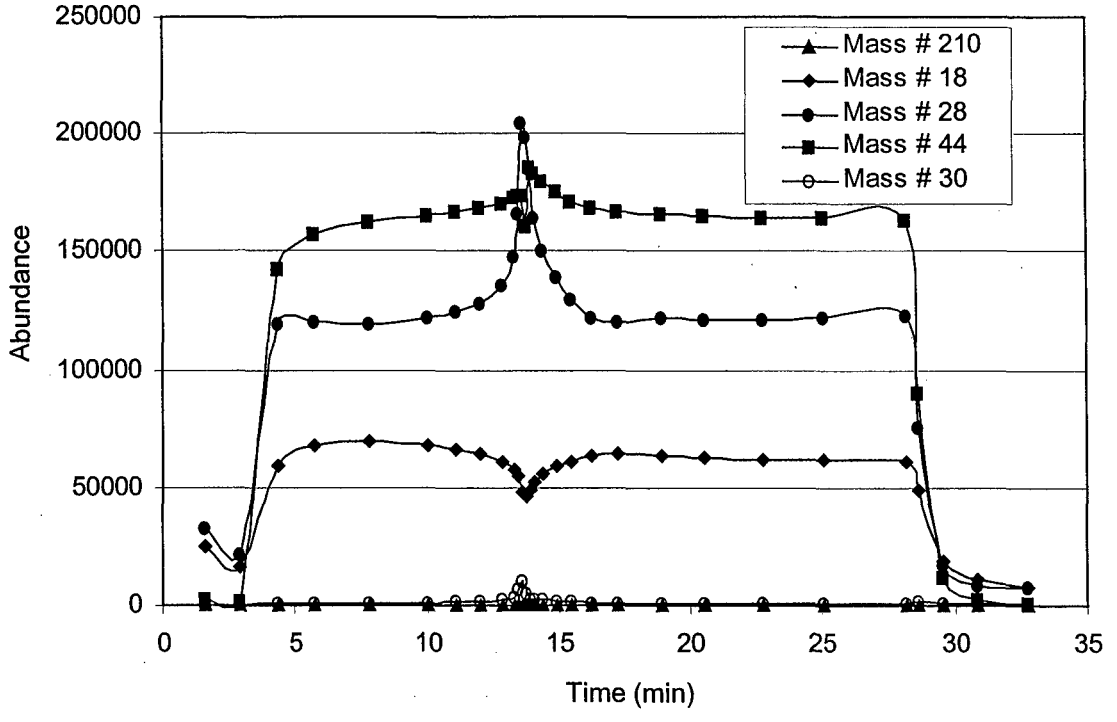

Figure 22. Product abundance versus time during O_2 plasma decontamination of TNT.

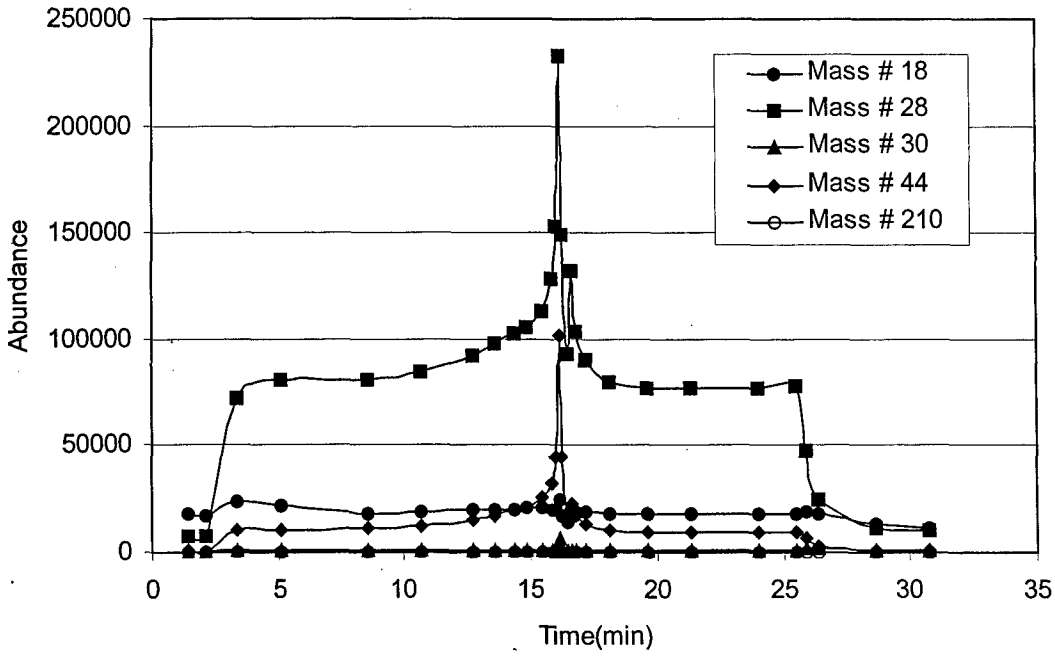

Figure 23. Product abundance versus time during H_2 plasma decontamination of TNT.

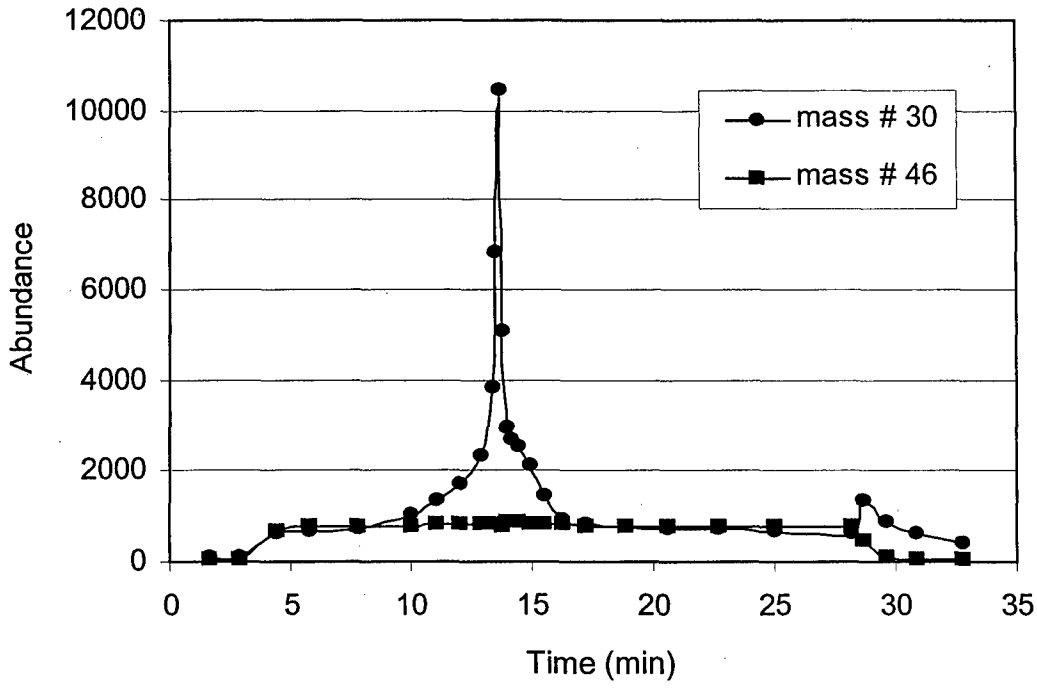

Figure 24. NO_x abundance versus treatment time during O_2 plasma decontamination of TNT.

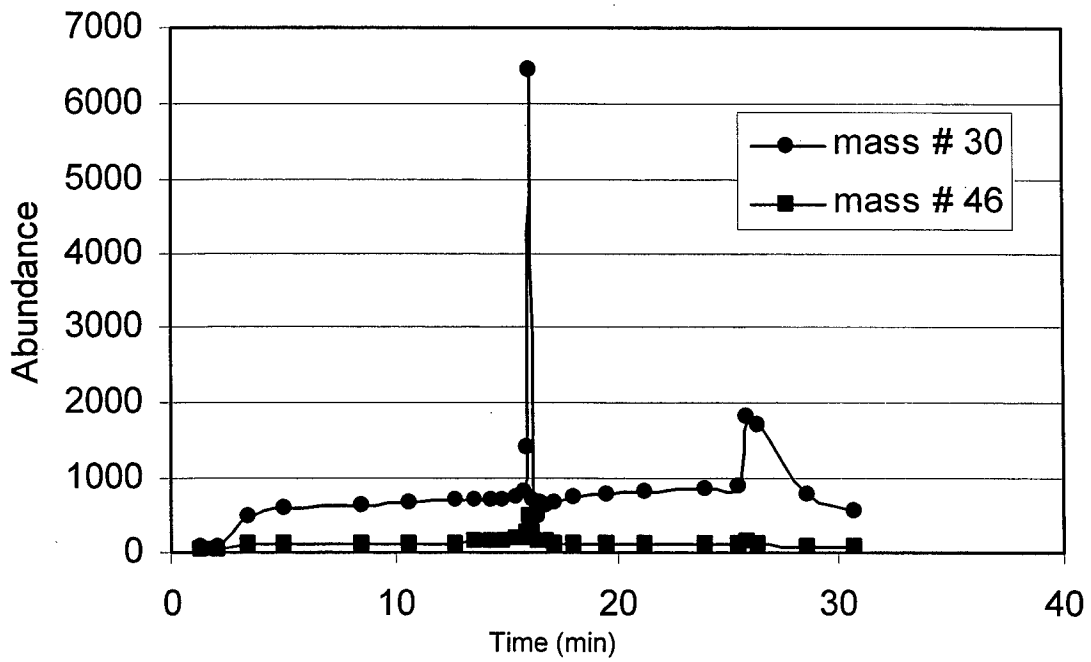

Figure 25. NO_x abundance versus treatment time during H_2 plasma decontamination of TNT.

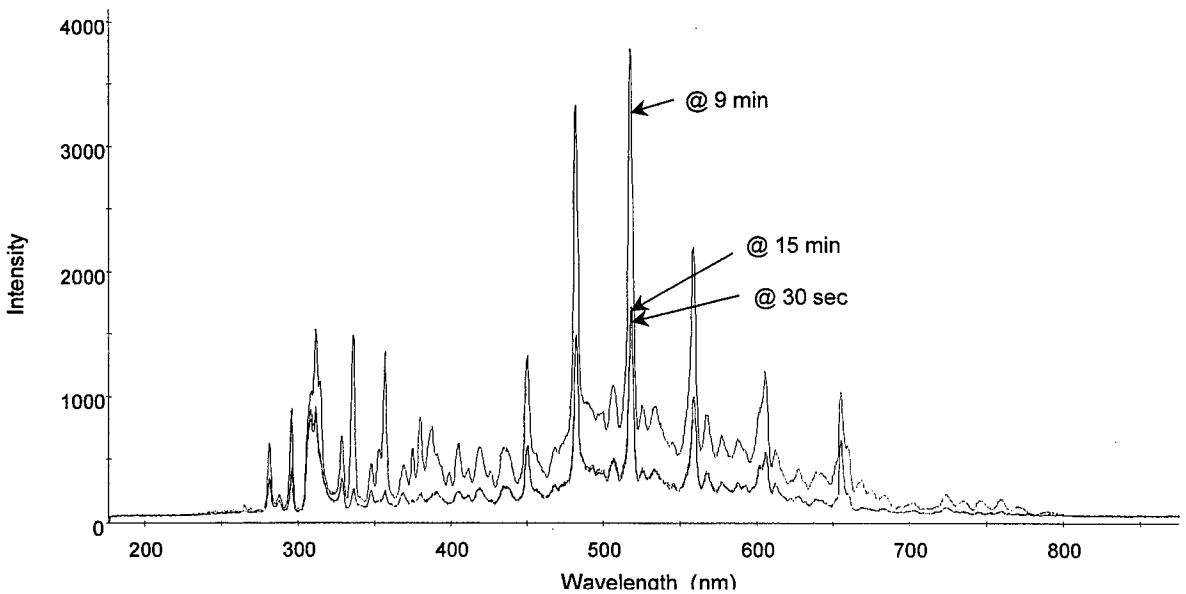

Figure 26. Emission spectra of H_2O plasma for decontamination of TNT, 200 W, CW.

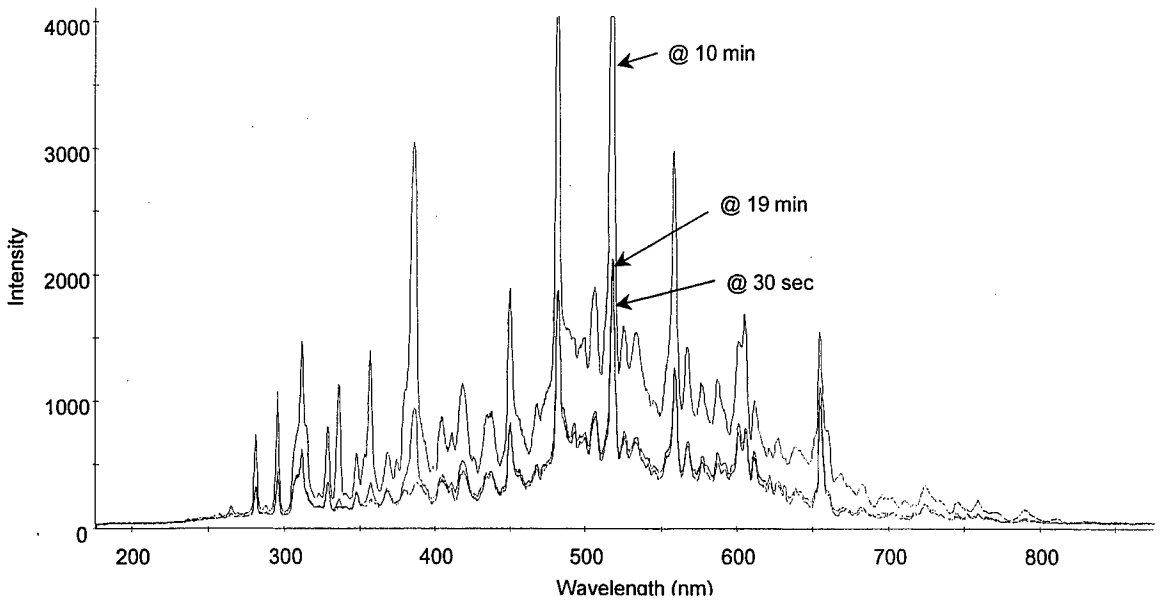

Figure 27. Emission spectra of H_2 plasma for decontamination of TNT, 200 W, CW.

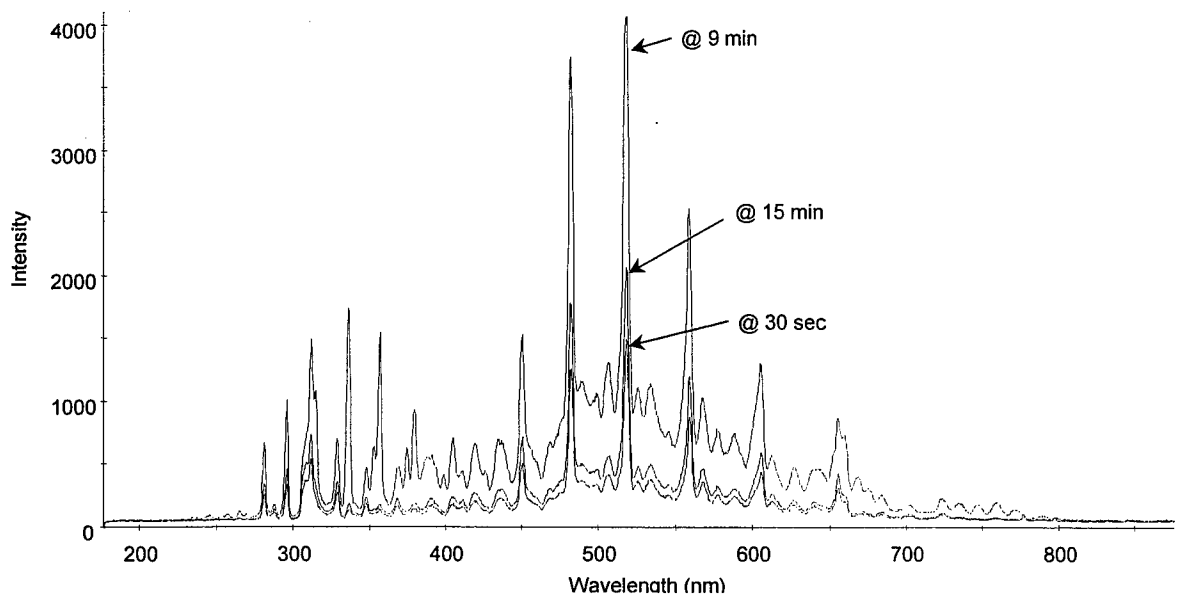

Figure 28. Emission spectra of O_2 plasma for decontamination of TNT, 200 W, CW.

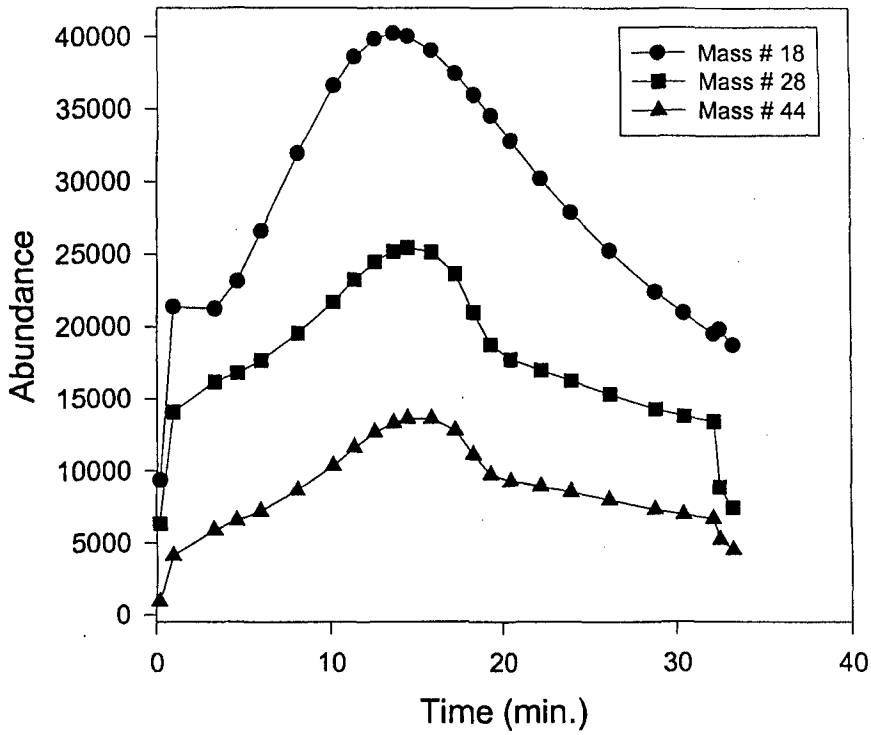

Figure 29. Product abundance versus time during O_2 plasma decontamination of RDX.

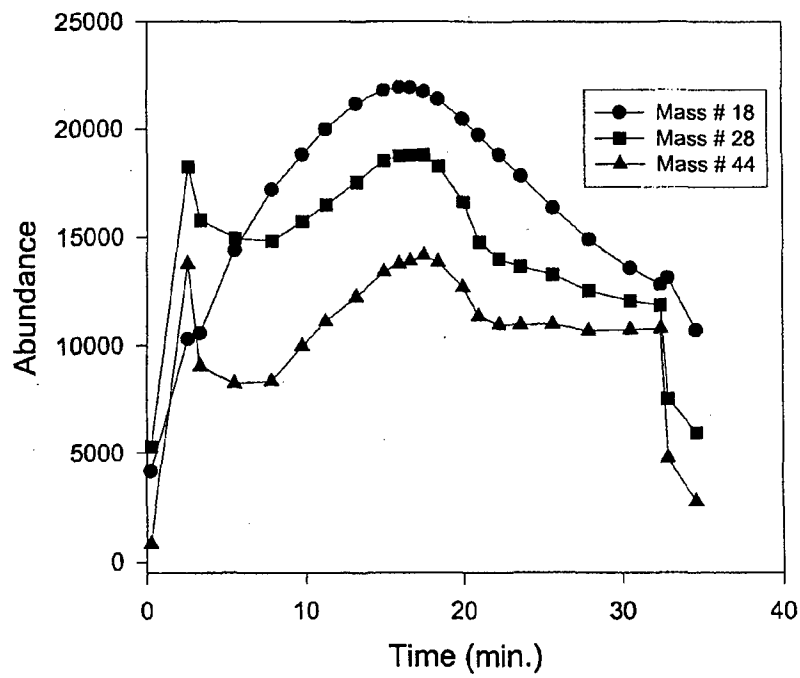

Figure 30. Product abundance versus time during H_2 plasma decontamination of RDX.

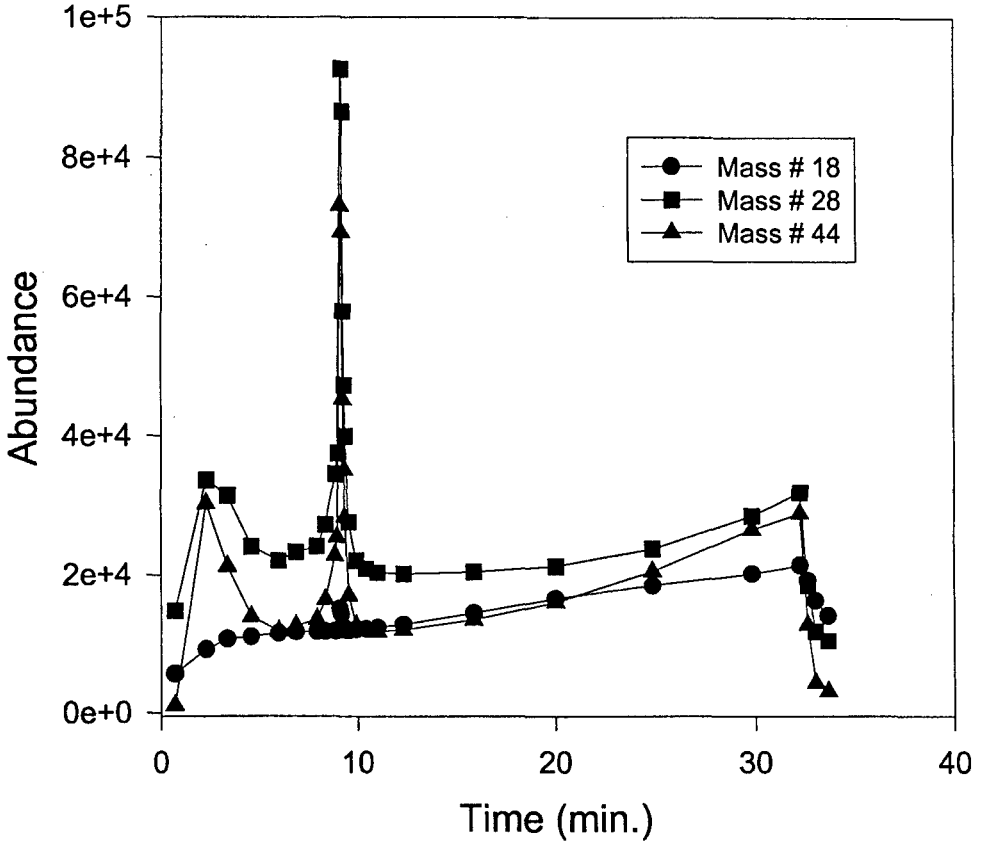

Figure 31. Product abundance versus time during O_2 plasma decontamination of TNT.

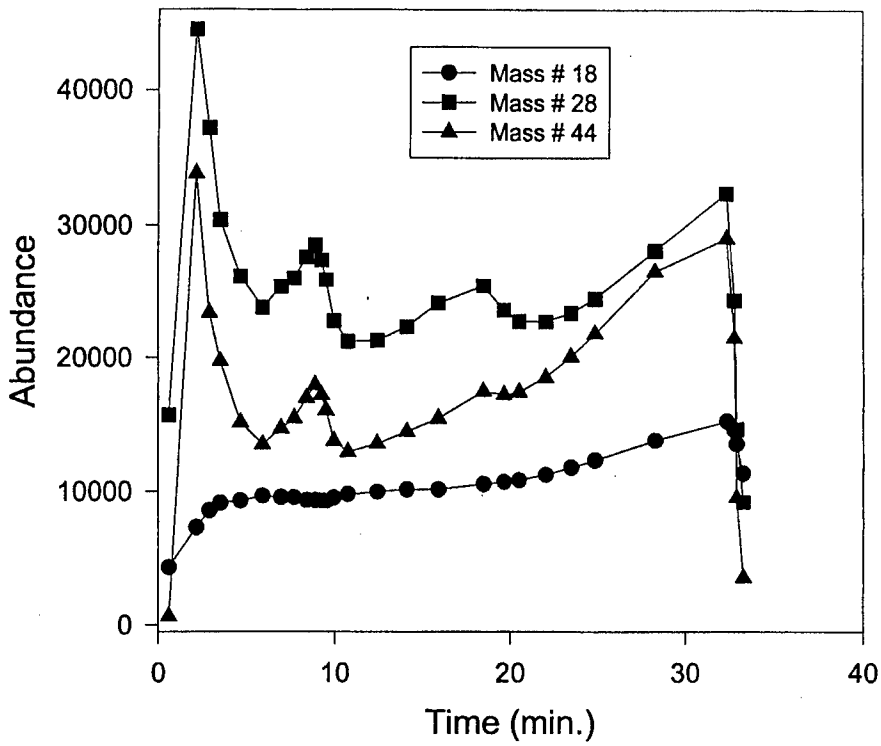

Figure 32. Product abundance versus time during O_2 plasma decontamination of Comp B.

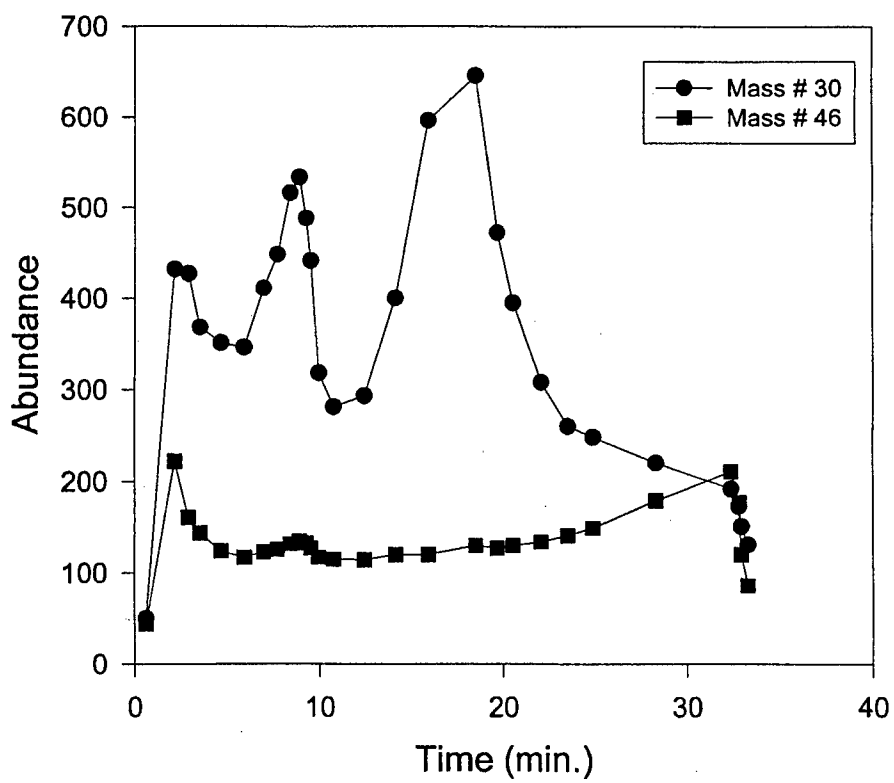

Figure 33. Product abundance versus time during O_2 plasma decontamination of Comp B.

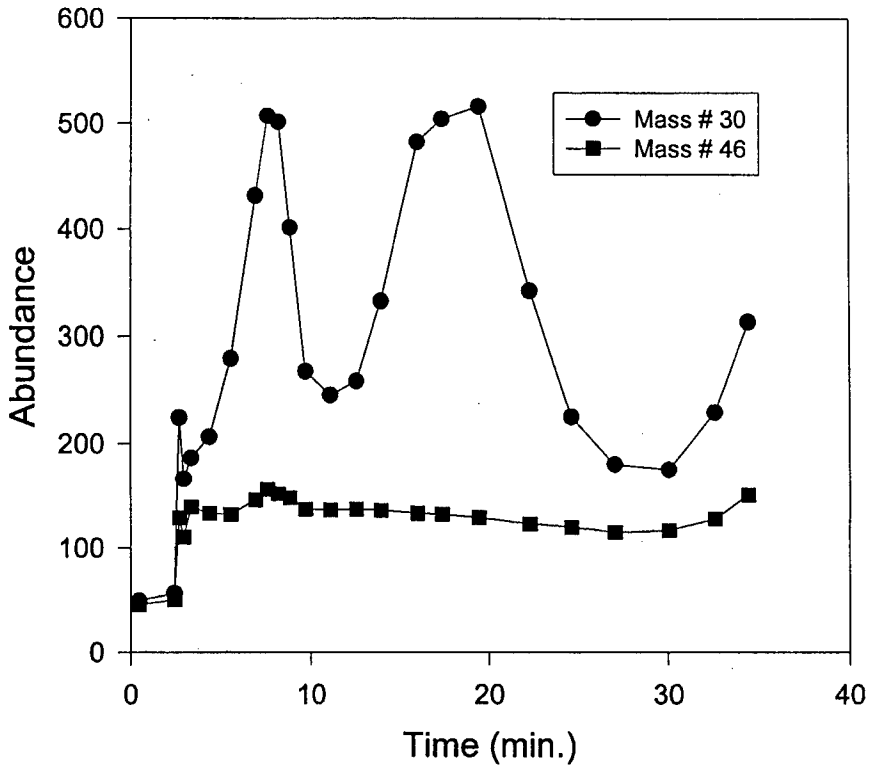

Figure 34. Product abundance versus time during O_2 plasma decontamination of Comp B.

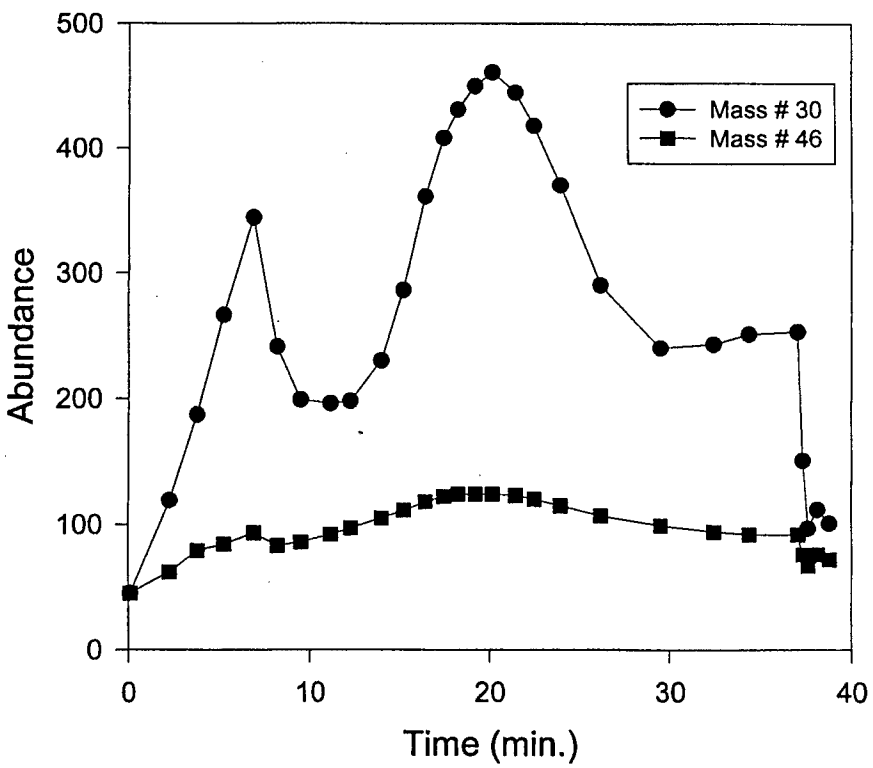

Figure 35. Product abundance versus time during H_2 plasma decontamination of Comp B.

LIST OF PUBLICATIONS AND PRESENTATIONS

B.W.-L. Jang, J.J. Spivey, R.B. Timmons, and L. Sotsky, "Non-thermal Plasma for Decontamination of Artillery Shells," presented at the 1999 Global Demil Symposium, Tulsa, OK, May 17-20, 1999.

B.W.-L. Jang, J.J. Spivey, C. Savage, R.B. Timmons, L. Sotsky and S. Levy, "Non-thermal Plasma for Decontamination of Artillery Shells," presented at the "Partners in Environmental Technology" Technical Symposium and Workshop, Arlington, VA, Nov. 30 – Dec. 2, 1999.

B.W.-L. Jang, and J.J. Spivey, "Catalytic Hydrodesulfurization and Hydrodechlorination of Chloroethyl Ethyl Sulfide"; *Catalysis Today* 55, p. 3-10, 2000.

B.W.-L. Jang, R.B. Timmons, and L. Sotsky; "Decontamination of Artillery Shell Casings with RF Nonthermal Plasma," presented at the 2000 Global Demil Symposium, Coeur d'Alene, Idaho, May 15-18, 2000.

B.W.-L. Jang, C.R. Savage, R.B. Timmons, S. Levy and L. Sotsky, "Environmental Benign and Economical Decontamination of Artillery Shell Casings with RF Non-thermal Plasma," presented at the Partners in Environmental Technology Technical Symposium and Workshop, Arlington, VA, Nov. 28–Dec. 1, 2000.

B.W.-L. Jang, "Low Pressure RF Plasma for Surface Decontamination of Artillery Shell Casings." Submitted to *Industrial Engineering and Chemistry Research*.

B.W.-L. Jang, K.A. Frankel, J.J. Spivey, and R.B. Timmons, "Hydrodechlorination of 1,1,1 Trichloroethane over Metal Supported Catalysts," presented at the AIChE National Meeting at Houston, Texas, March 1997.

B.W.-L. Jang, K.A. Frankel, J.J. Spivey, and R.B. Timmons, "Catalytic Hydrodesulfurization and Hydrodechlorination of Chloroethyl Ethyl Sulfide," presented at the ACS National Meeting at Las Vegas, Nevada, September 1997, and published in the preprints of the Division of Petroleum Chemistry of ACS, Vol. 42, No. 3, p. 615-618, 1997.

K.A. Frankel, B.W.-L. Jang, G.W. Roberts, and J.J. Spivey, "Deactivation of 3%Pt/Alumina for Hydrodechlorination of 1,1,1 Trichloroethane." Published in *Catalyst Deactivation*, Studies in Surface Science and Catalyst Series, Vol. 111, p. 239-250,1997.

B.W.-L. Jang, K.A. Frankel, J.J. Spivey, and R.B. Timmons, "Hydrodesulfurization and Hydrodechlorination of Chloroethyl Ethyl Sulfide," presented at the ACS National Meeting at Dallas, March 1997, and published in the preprints of the Division of Petroleum Chemistry of ACS, Vol. 43, No. 1, p. 83-86 (paper attached), 1998.

Frankel, K.A., B.W.-L. Jang, G.W. Roberts, and J.J. Spivey, "Deactivation of Hydrodechlorination Catalysts: I-Experiments with 1,1,1-Trichloroethane," Appl. Catal., Vol. 205, 2001.

Frankel, K.A., B.W.-L. Jang, G.W. Roberts and J.J. Spivey, "Deactivation of Hydrodechlorination Catalysts: II Experiments with 1,1,1-Dichloroethane and 1,1-Dichloroethane," Appl. Catal., in press.

SCIENTIFIC PERSONNEL

K.A. Frankel received a Ph.D. degree in Chemical Engineering from North Carolina State University in December 1997.

R. Mitchell received a M.S. degree in June 1997 and S. Vasquez received a Ph.D. in Applied Chemistry in December 1997 from University of Texas-Arlington.

B. Thomas received a M.S. degree in Engineering from the University of Texas-Arlington (UTA) in August 1998.